Geomorphology 114 (2010) 415–430

Contents lists available at ScienceDirect

Geomorphology

journal homepage: www.elsevier.com/locate/geomorph

Timing and controls on late Quaternary landscape development along the eastern Sierra El Mayor range front in northern Baja California, Mexico

Phillip A. Armstrong [a,*], Rene Perez [a,1], Lewis A. Owen [b], Robert C. Finkel [c]

[a] Department of Geological Sciences, California State University Fullerton, Fullerton, CA 92831 USA
[b] Department of Geology, University of Cincinnati, Cincinnati, OH 45221-0031, USA
[c] Lawrence Livermore National Laboratory, Livermore, CA 94550, USA

ARTICLE INFO

Article history:
Received 10 February 2009
Received in revised form 17 August 2009
Accepted 18 August 2009
Available online 31 August 2009

Keywords:
Colorado River delta
Tectonics
Terraces
Climate
Optically stimulated luminescence
Terrestrial cosmogenic nuclides
Uplift

ABSTRACT

The Sierra El Mayor–Sierra Cucapá mountain range in northern Baja separates the Colorado River delta from the Laguna Salada Basin and is important in terms of understanding the structural transition from the northern Gulf Extensional Province to the San Andreas system. One of the principal Quaternary landscape features of the eastern Sierra El Mayor–Sierra Cucapá is a prominent surface that slopes ~1–2° eastward towards the Colorado River Delta. Along the eastern side of the Sierra El Mayor and facing the Colorado River delta, but not along other piedmont mountain fronts that face the delta, this surface is terminated by a series of stepped terrace surfaces. The terrace surfaces are cut into fluvial–deltaic deposits from the Colorado River delta system and are capped by ~1 m thick gravels. Optically stimulated luminescence ages from interbedded coarse sands in the capping gravels of the upper surface and two of the inset terraces range from ~17 to 31 ka (average 24±3 ka) but lack a systematic age trend from upper to lower surface. The underlying fluvial–deltaic deposits have older optically stimulated luminescence ages of 31 to 39 ka and suggest Colorado River delta deposition during the relatively stable interstadial of the Middle Wisconsinan substage (Marine Isotope Stage 3) when sea level was ca −60 to −80 m. Samples from depth-profiles in the capping gravels and from the top of the upper surface have a mean ^{10}Be terrestrial cosmogenic nuclide age of 59±5 ka. When corrected for inheritance, an average age of ~21 ka is computed for exposure of the capping gravels on the upper surface and inset terraces, which is in the range of the optically stimulated luminescence burial ages. Both the upper surface and inset terraces formed 17–30 ka at a transition time from dry to relatively wet climate when increased aggradation caused alluvial fan development on the upper surface. Regionally, these surfaces correlate with the Q2c–Q3a age deposits of the southwestern North America alluvial fan and terrace deposits. Sea level was also falling rapidly at this time, which may have caused the Colorado River to become entrenched near the range front thus allowing rapid response and down-cutting to form the inset terraces on the east side of the Sierra El Mayor facing the delta. Assuming the 34 ka delta deposits graded to a base level that was −60 to −80 m during Marine Isotope Stage 3, the computed surface uplift rate for the eastern side of the Sierra El Mayor is ~2.1–2.7 mm/yr. This uplift may be accommodated on a fault or fault system that is a southward extension of the Mexicali spreading and seismic zone that is buried beneath the Colorado River delta east of the Sierra El Mayor. The uplift rates from this study are consistent with geologic and geodetic data for the Sierra El Mayor and Sierra Cucapá, and account for much of the missing extensional strain across the area.

Published by Elsevier B.V.

1. Introduction

The Sierra El Mayor and Sierra Cucapá form a northwest-trending mountain range that separates the Colorado River delta from the below sea level Laguna Salada Basin to the west (Figs. 1 and 2). They are located within the northern Gulf Extensional Province (Gastil et al., 1975) that extends the length of the Gulf of California and merges to the north with the San Andreas fault system in southern California (Fig. 1). The sierras El Mayor and Cucapá are located just west of the right-lateral Cerro Prieto fault and Mexicali seismic zone (Fig. 2). The Cerro Prieto fault, a major transform fault, and the Mexicali seismic zone outline a spreading center (Frez and González, 1991) that accommodates most of the North American–Pacific Plate relative motion at this location (Bennett et al., 1996). Geodetic studies across the Laguna Salada–Sierra El Mayor area suggest extension rates of 2–4 mm/yr (Savage et al., 1994), but only about 40% of this strain can be accounted for at 10^4–10^6 year timescales (Axen et al., 1999, 2000). Much of the evidence of this strain deficit may be obscured by

* Corresponding author. Tel.: +1 657 278 3169; fax: +1 657 278 7266.
E-mail address: parmstrong@fullerton.edu (P.A. Armstrong).
[1] Present address: Hromadka & Associates, Rancho Santa Margarita, CA, 92688, USA.

0169-555X/$ – see front matter. Published by Elsevier B.V.
doi:10.1016/j.geomorph.2009.08.005

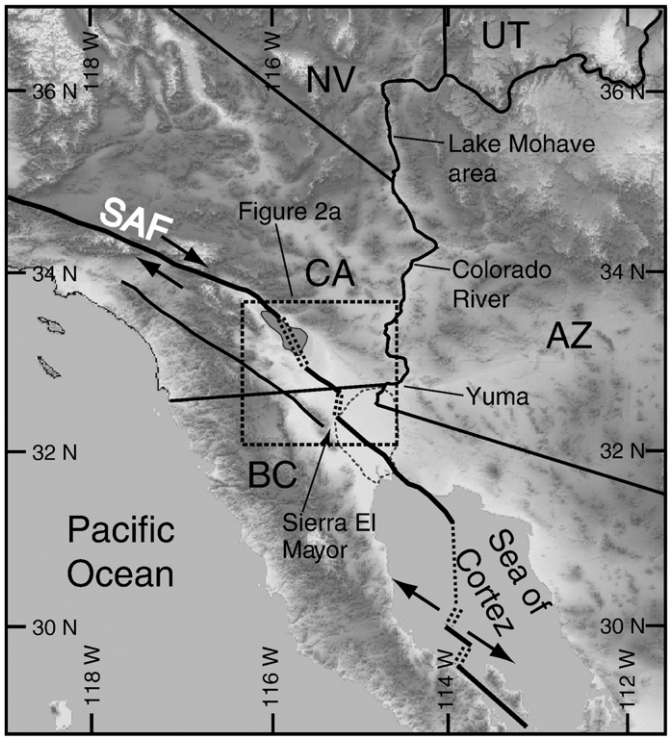

Fig. 1. Location map showing the generalized major structures associated with the transition from the northern Gulf Extensional Province to the San Andreas Fault (SAF) transform system. Note that the Sierra El Mayor study area is located in the middle of this transition. Bold lines are strike-slip faults and the dotted lines between the strike-slip faults are general locations of extensional zones. The arrows show relative motion across the strike-slip faults and across the spreading centers in northern Sea of Cortez. CA is California, AZ is Arizona, NV is Nevada, UT is Utah, BC is Baja California.

the Colorado River delta deposits on the east side of the Sierra El Mayor and Sierra Cucapá mountain system. Thus, the study of the relations between the deposits and terraces along the eastern Sierra El Mayor and the tectonic uplift that can be inferred from them may provide important new constraints on how strain is partitioned along this major tectonic system.

Most of our understanding of the Quaternary landscape development and timing for southwestern North America comes from the Mojave Desert region of the Great Basin and is based primarily on geomorphic expression and soil characteristics (e.g., Bull, 1991). The Mojave Desert region chronology has been correlated with or utilized in many studies throughout the desert southwest USA area (e.g., Wells et al., 1987; Bull, 2000; Klinger, 2001, 2002; Knott et al., 2005; Bull, 2007; Frankel et al., 2007; Sohn et al., 2007). Most of the process–response models for the Mojave Desert region suggest that alluvial fan aggradation is due to changes from wet to dry (glacial to interglacial) periods whereby factors such as reduced vegetation and increased exposure of soil to erosion cause increases in sediment supply and fan aggradation (e.g., Wells et al., 1987; Bull, 1991). Alternatively, fan aggradation could occur during transition from dry to wet periods (Harvey et al., 1999a,b). In this case, increased runoff during wetter periods drives fan aggradation, especially in areas where climate is relatively arid even during glacial periods. Therefore, understanding the timing of fan aggradation with respect to major climatic changes is critical for understanding the processes of fan formation. Recently, Spelz et al. (2008) used terrestrial cosmogenic nuclide ages and morphologic characteristics of fan surfaces on the western side of the Sierra El Mayor to make correlations with regional fan ages to suggest that fans there formed during a dry to wet transition. However, the Spelz et al. (2008) study only had two absolute ages from which to constrain the timing of alluvial fan formation. Thus, study of alluvial fan timing and development from the eastern side of the Sierra El Mayor (this study) could provide additional important age constrains on and insights into the interactions between climate and alluvial fan formation in this region.

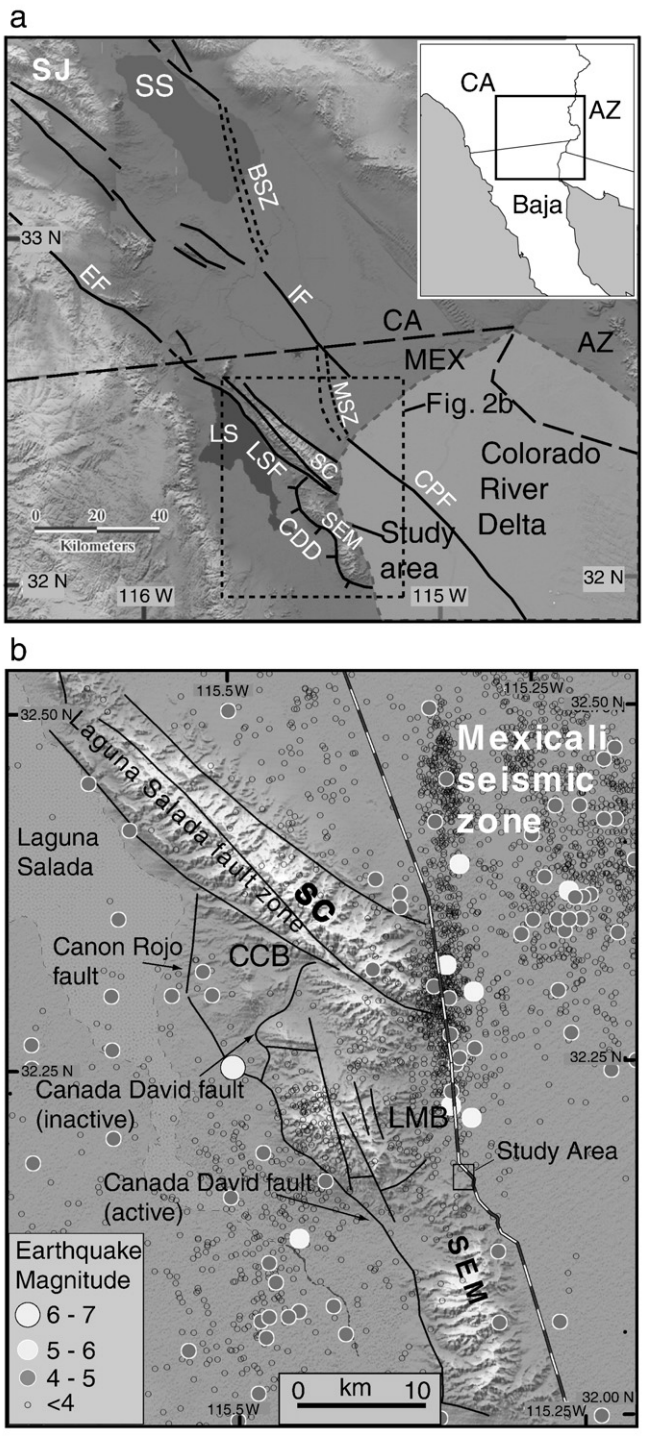

Fig. 2. Location maps showing (a) location of Sierra El Mayor (SEM)–Sierra Cucapá (SC) range system between the Colorado River delta and the Laguna Salada (LS) and (b) locations of the major faults near the study area, which is located on the east side of the Sierra El Mayor. CA is California, AZ is Arizona, Mex is Mexico, SJ is the San Jacinto Mountains, SS is the Salton Sea, EF is the Elsinore fault, LSF is the Laguna Salada fault, CPF is the Cerro Prieto fault, IF is the Imperial fault, CDD is the Cañada David Detachment, BSZ is the Brawley spreading zone, MSZ is the Mexicali spreading zone, LMB is the Lopez Mateos basin, CCB is the Cerro Colorado basin. In (b), circles show seismicity from 1932 to 2006 from Southern California Earthquake Center catalog. The black-white line on east side of SEM and SC is Mexico Highway 5.

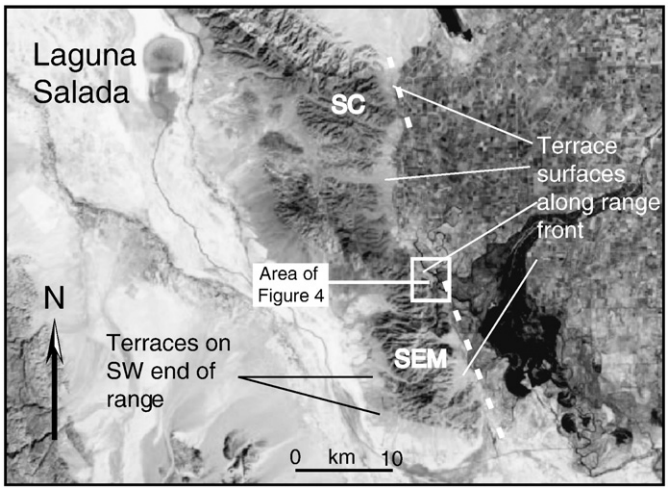

Fig. 3. Landsat7 image showing the locations of upper surface and inset terraces on the east and southwest sides of the Sierra El Mayor. White dashed line along the eastern range front shows the approximate location of an inferred fault. Note the embayed nature of the east side of the range front between the inferred fault traces.

The eastern side of the Sierra El Mayor faces the Colorado River delta (Fig. 1) and therefore the Quaternary landscape features there were at least partially controlled by factors that caused changes in the delta. These factors may include climate-induced discharge changes, base-level changes in the nearby Sea of Cortez, and tectonics. The principal Quaternary landscape features of the eastern side of the range, and the focus of this paper, are a series of alluvial fan surfaces that formed on top of and cut into the Colorado River delta deposits. Detailed and insightful work by Carter (1977) on similar strata and surfaces around the south end of the Sierra El Mayor led him to propose several possibilities for the genesis of those surfaces including tectonic uplift, changes in base level due to Colorado River entrenchment, and/or climate change. However, Carter (1977) was hindered by the lack of reliable age data for the surfaces in the southern Sierra El Mayor.

In this paper, we describe and evaluate a range-front upper surface and a set of at least four stepped terrace surfaces that are located along much of the eastern side of the Sierra El Mayor and southeastern end of the Sierra Cucapá where both face the present Colorado River delta and floodplain (Figs. 2–4). We also provide age constraints on these features that allow us to interpret their genesis and their relations to climate and sea-level change, Colorado River entrenchment, and tectonic uplift associated with potential faults whose surface expression has been obscured by the Colorado River delta.

2. Geologic setting

The Sierra El Mayor–Sierra Cucapá is located at the highly deformed and active structural transition from the northern Gulf Extensional Province to the San Andreas system. Geodetic studies (Savage et al., 1994) and geologic studies (Mueller and Rockwell, 1995; Axen et al., 1999; Dorsey and Martin-Barajas, 1999; Axen et al., 2000; Spelz et al., 2008; Fletcher and Spelz, 2009) show that the range has experienced rapid extension and uplift during the Quaternary. All of these geologic studies focused on faults and other geologic features on the west side of the range where Quaternary deposits are cut by numerous faults of the Laguna Salada, Cañon Rojo, and Cañada David detachment fault systems (Fig. 2). The main fault on the western side of the Sierra El Mayor is the west-dipping Cañada David detachment fault (Siem and Gastil, 1994; Axen and Fletcher, 1998), which extends for more than 45 km along the western range front (Axen and Fletcher, 1998; Fletcher and Spelz, 2009) and places Miocene to Pleistocene sediments on top of Mesozoic crystalline basement rocks (Siem and Gastil, 1994; Axen and Fletcher, 1998; Dorsey and Martin-Barajas, 1999; Martin-Barajas et al., 2001). Low-temperature thermochronology data indicate that the Cañada David detachment has accumulated ~12 km of horizontal displacement in the last ~12 Ma, indicating an extension rate of ~1 mm/yr (Axen et al., 2000). An extensive array of faults that cut Quaternary alluvial fan surfaces is present along the entire length

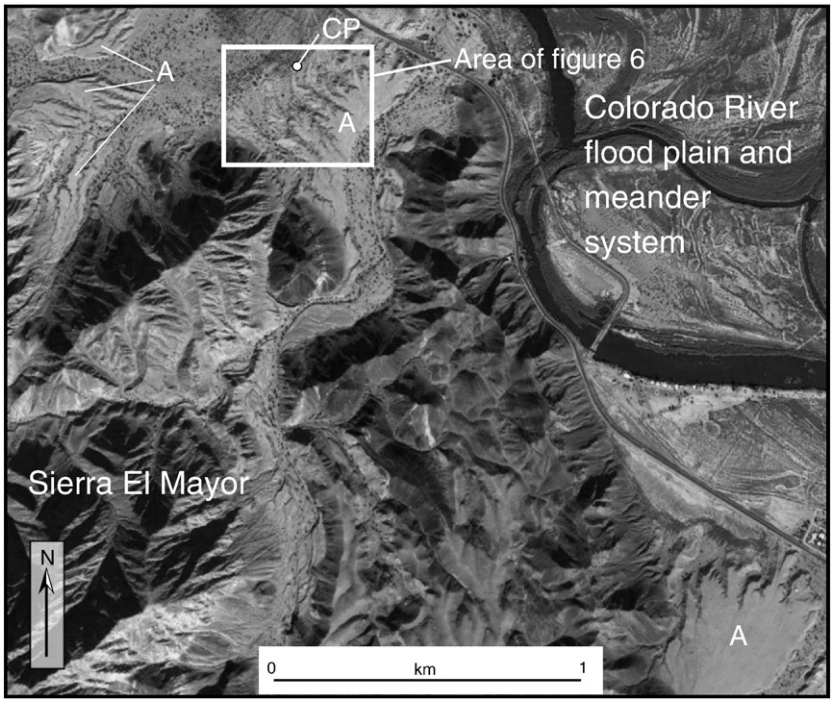

Fig. 4. Google Earth image with locations of mapped upper surface and inset terraces. The areas marked with "A" are exposures of terrace surfaces evaluated in this study. CP is location of control point shown in Fig. 6.

of the western Sierra El Mayor mountain front and in the hanging wall of the Cañada David detachment fault. These faults are thought to represent surface ruptures related to slip on the low-angle Cañada David detachment (Axen et al., 1999; Fletcher and Spelz, 2009). The Cañada David detachment fault ends at the near-vertical normal-dextral Laguna Salada fault to the north (Fig. 2), which has been active in the Holocene and is thought to have ruptured in 1892 (Mueller and Rockwell, 1995).

The eastern side of the Sierra El Mayor–Sierra Cucapá, especially the Sierra El Mayor, faces the Colorado River delta (Figs. 2 and 3) and is directly adjacent to the modern river meander system. Whereas active faults are present along most of the west side and northern parts of the Sierra El Mayor–Sierra Cucapá (Spelz et al., 2008), no active faults have been mapped at the surface on the east side where the erosional and depositional effects of the Colorado River have sculpted the range front. It is possible that faults exist on the eastern flank of the Sierra El Mayor, but they are buried under Holocene fluvial-deltaic deposits. The main faults to the east, but far from the eastern Sierra El Mayor–Sierra Cucapá range front, are the right-stepping *en echelon* dextral-slip Cerro Prieto and Imperial faults and the Mexicali seismic zone; the Cerro Prieto fault is located ~10–20 km from the eastern side of the Sierra El Mayor–Sierra Cucapá range front (Fig. 2). This region represents a major partitioned transform fault and extensional spreading center system (Frez and Gonzalez, 1991; Axen et al., 2000) that accommodates most of the modern motion between Pacific and North American plates at this latitude (Bennett et al., 1996).

The Sierra El Mayor–Sierra Cucapá bedrock consists mostly of a complex group of Paleozoic metamorphic and Mesozoic granitic rocks (Gastil et al., 1975; Todd et al., 1988; Siem, 1992). The metamorphic rocks consist of biotite schist, migmatitic gneiss, amphibolite, marble, and quartzite. The granitic rocks generally consist of very coarse-grained granodiorite and tonolite. The metamorphic and granitic rocks are cross-cut by white quartz veins throughout the range. The basement rocks mostly are overlain by or are in fault contact with Mio-Pliocene to Pleistocene alluvial, fluvial, and marine strata in exhumed Cerro Colorado and Lopez Mateos basins (Vazquez-Hernandez et al., 1996; Axen and Fletcher, 1998; Axen et al., 1998; Dorsey and Martin-Barajas, 1999) north and west of the study area (Fig. 2). The stratigraphy of these basins generally consists of marine mudstone and fine sand units of the Mio-Pliocene Imperial Formation. The Imperial Formation is unconformably overlain by non-marine Pliocene–Pleistocene conglomerates, breccias, and conglomeratic sandstone. The non-marine sequence is typically red and is referred to by Dorsey and Martin-Barajas (1999) collectively as the "red bed sequence". The Plio-Pleistocene Palm Springs formation, which interfingers with the red bed sequence, consists of fine-grained sandstone, siltstone, and mudstone and is interpreted to represent ancestral Colorado River fluvial and deltaic deposits (Vazquez-Hernandez et al., 1996; Winkler and Kidwell, 1996; Axen et al., 1998; Dorsey and Martin-Barajas, 1999).

The underlying deposits into which the terrace surfaces of this study are cut consist of a sequence of red interbedded clays, silts, sand, and gravel. The clay units are reddish brown, about 2 to 20 cm thick, and contain abundant gypsum and caliche. Silt units are tan to reddish brown, interfinger with clay and fine sand units, and are about 20 to 75 cm thick. The sand units are light brown to reddish brown, fine- to coarse-grained, poorly- to well-sorted, and locally contain minor gravel, silt, and clay interbeds and local carbonate nodules. The sand layers coarsen and thicken toward the range front and generally are planar bedded but locally form channelized bases that are up to 0.25 m deep and up to 2 m wide. Gravels are rare away from the range front, but interfinger with the finer deposits and become more prominent toward the range front. Gravels typically grade upward to finer sands within the red beds and are composed of poorly sorted subangular clasts of mostly granodiorite, tonalite, biotite schist, and vein quartz, indicating a nearby source from the basement rocks of the Sierra El Mayor. We, as well as Carter (1977), interpret the clay, silt, and sand deposits of these "red bed" deposits to be fluvial–deltaic deposits from the Colorado River with interfingering gravel deposits derived from local basement exposures. Carter (1977) obtained one U-series age of 40–60 ka from a paleosol in similar deposits from the south end of the Sierra El Mayor. Carter (1977) interpreted this age as a minimum age and that these sediments were deposited during the Colorado River deposition ~120 ka during relative sea level high stand. Thus, the red bed deposits in this study appear to be the younger upward continuation of ancestral Colorado River fluvial–deltaic deposition of the Plio-Pleistocene red bed sequence and Palm Springs Formation described above.

3. Geomorphological setting

One of the principal Quaternary landscape features of the Sierra El Mayor and Sierra Cucapá, as well as other ranges farther south that face the Colorado River Delta and Gulf of California, is an alluvial plain surface (as defined by Ritter et al. (2002) and references therein) that extends basinward from the mountain fronts. In most locations, this surface is truncated to form an escarpment that is about 10–15 m above the Colorado River delta floodplain and that slopes upward to the range front to heights of about 25–30 m above the floodplain. Along the entire eastern side of the Sierra El Mayor facing the Colorado River delta, the aggradational alluvial plain surface (referred to as 'upper surface' later in text) is terminated basinward by a series of at least four stepped terrace surfaces (Fig. 5). These steps are noticeably absent along other ranges that face the delta. Along the eastern Sierra El Mayor, the terrace steps are extensive and well-formed at mountain-front embayment and canyons and they are short and poorly developed where basement salients face the delta.

Spelz et al. (2008) described eight alluvial fan surfaces on the west side of the Sierra El Mayor facing the Laguna Salada (Fig. 2). Based on two terrestrial cosmogenic nuclide ages and regional correlations, they interpret these alluvial fan surfaces to range in age from modern active fan (their Q1) to >204 ka (their Q8). These alluvial fan deposits are dominated by coarse-grained debris flow deposits and fluvial deposits. Correlations of the fans and relative ages were made on the basis of relative elevations, rock varnish development, bar and swale morphology, weathering of surface clasts, vegetation changes, and soil development. Unlike the alluvial fan deposits and surfaces on the east side of the Sierra El Mayor, the fans on the west side are cut by an extensive array of fault scarps along almost the entire length of the range (Spelz et al., 2008; Fletcher and Spelz, 2009). Spelz et al. (2008) show that the fans on the west side of the range formed from an integrated and complex climate-tectonic response where fan growth was controlled mainly by tectonic activity, but modulated as hydrologic conditions that changed in response to Milankovitch timescale climatic changes.

Our study area is located at the south end of an approximately 15 km-wide arc-shaped embayment in the central to northern part of the eastern side of the Sierra El Mayor (Fig. 3). We focus on a relatively small region (~1 km^2) (Fig. 4) to evaluate timing and genesis of these geomorphic features. Though the upper surface and terraces are present along most of the eastern Sierra El Mayor, the surficial capping gravels, underlying fluvial–deltaic deposits, and relevant surficial geomorphic characteristics are especially well preserved in the study area (Fig. 5).

4. Modern climate

The Sierra El Mayor is located in the Sonoran Desert and has a modern climate that is extremely arid. According to the updated Köppen–Geiger climate classification scheme (Peel et al., 2007), the Sierra El Mayor area is considered a hot desert environment. Spelz

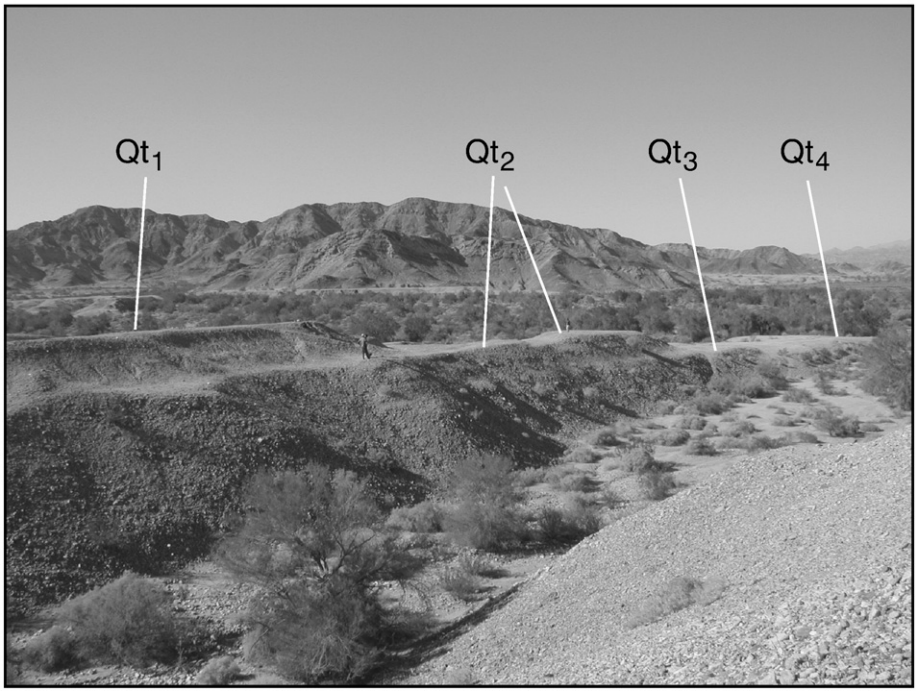

Fig. 5. View of terrace surfaces looking towards the northwest. Four terraces (Qt1–Qt4) are labeled to illustrate their relative elevations. Person for scale on Qt2 surface. Location of this terrace spur is shown on Fig. 6. Note the additional terrace surfaces at the base of the range in the background.

et al. (2008) report mean annual temperatures of 22.1 to 24.4 °C and mean annual precipitation of 54.9 to 127.4 mm/yr based on weather stations in the Laguna Salada area. Analysis of data from one weather station located ~50 km north of the study area, but on the east side of the Sierra El Mayor–Sierra Cucapá mountains indicate mean annual temperature and precipitation of 22.6 °C (20.0 to 24.1 °C) and 63.4 mm/yr (6.3 to 196.2 mm/yr), respectively, for the years 1951–2009. The Sierra El Mayor area is in the rain shadow of the ~2000 m high Sierra Juárez and Peninsular Range to the west and the westerly storm-track precipitation from the Pacific Ocean is effectively cut off. Most precipitation comes in the late summer months as monsoonal moisture is carried northward from the Gulf of California.

5. Approach and methods

Several methods were employed to assess the geologic, geomorphic, and age relations of the upper surface, terraces, and their deposits. The geomorphology of the study area was assessed using total station mapping, local oblique aerial photograph analysis, and general field mapping at scale of approximately 1:3000. A topographic map (Fig. 6) was generated from the total station data from which elevation profiles could be extracted. Field elevations were tied to absolute elevations by differencing local base stations with a base station at Point Loma, CA and horizontal and vertical accuracies are 0.05 and 0.4 m, respectively.

In order to assess absolute ages of the upper surface and terrace, as well as the ages of the underlying fluvial–deltaic deposits, we employed the complimentary techniques of optically stimulated luminescence (OSL) and terrestrial in situ cosmogenic nuclide (TCN) dating. OSL dating is used to determine the time elapsed since a sediment sample was last exposed to daylight. Recent advancements in the OSL technique have made the technique more useful for dating fluvial and alluvial fan sediments (e.g., Stokes, 1999; Forman et al., 2000; Wallinga, 2002) and it has been successfully applied to these types of sediments in the western USA (e.g., Machette et al., 1992; Rockwell et al., 2000; Lee et al., 2001; Mahan et al., 2007; Sohn et al., 2007) and elsewhere (e.g., Forman and Pierson, 2002; Wallinga, 2002; Srivastava et al., 2003; Zhang et al., 2003; Hanson et al., 2004). OSL ages were obtained for alluvial sediments on the upper surface and terraces as well as the underlying fluvial–deltaic deposits. TCN dating is used to determine the time that a rock and/or sediment surface has been exposed to cosmic rays which have resulted in the production of terrestrial cosmogenic nuclides such as ^{10}Be and ^{26}Al by spallation (Gosse and Phillips, 2001). This technique has been successfully applied to dating exposure of alluvial fans in the western USA (e.g., Matmon et al., 2005, 2006; Frankel et al., 2007). TCN ages were obtained on depth profiles in the alluvial sediments, from surficial samples on the upper surface, and on clasts from modern drainages and hillslopes.

Soil development was evaluated on the upper surface and terraces to corroborate OSL and TCN ages. The soil development also allows correlation with and comparisons to regional alluvial fan chronologies. Soil correlation studies have been applied to many areas of the southwestern North America desert region (e.g., Wells et al., 1987; Bull, 1991; Mueller and Rockwell, 1995; Klinger, 2002; Frankel et al., 2007; Spelz et al., 2008).

6. Geomorphic analysis and results

The surfaces in the study area generally are preserved as spurs (Fig. 5) that extend northward in an arc-shaped pattern corresponding to the incised gullies that are trying to reach base level in the delta floodplain to the east of the Sierra El Mayor (Fig. 6). Along other parts of the eastern Sierra El Mayor it is notable that the surface spurs extend in other directions depending on local mountain front morphology. The tops of the lower inset surfaces are best preserved at the ends of the spurs, but the inset surfaces are preserved locally up the sides of the spurs (Fig. 5) or are preserved as isolated remnants (Fig. 6). Active drainages between the spurs grade to the active floodplain. Height differences between the surfaces are typically <1 m to about 2.5 m and the sub-parallel upper and inset surfaces slope 1–2° basinward (Fig. 7). The inset terraces below the upper surface appear to be straths (erosional surfaces) that are incised into the underlying fluvial–deltaic red bed deposits.

The upper surface and all the incised terrace surfaces are capped by 0.5 to 1.5 m-thick veneer of matrix- and cobble-supported, poorly

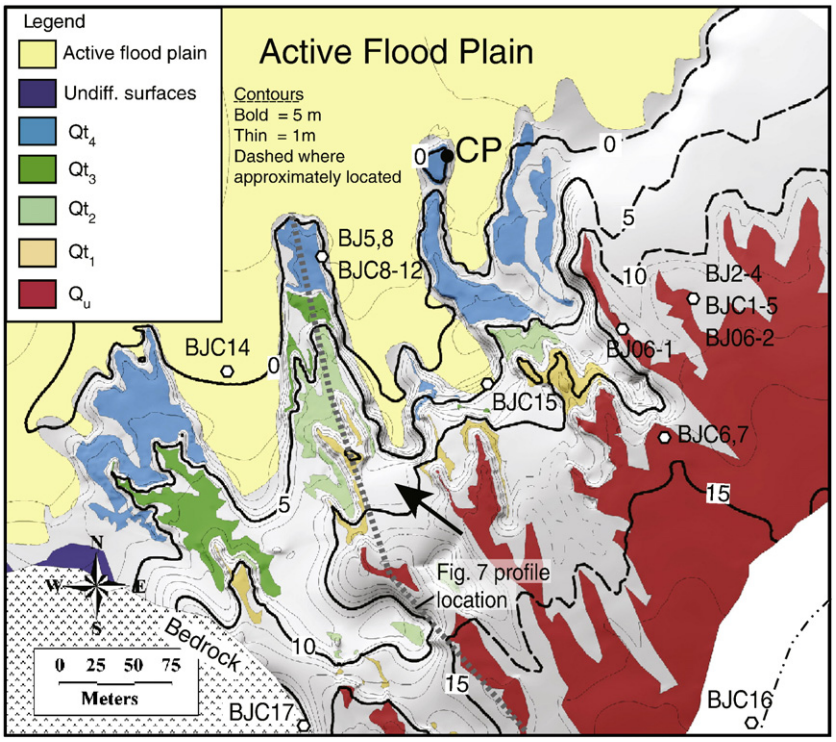

Fig. 6. Topographic map showing the distribution of upper surface and terraces in study area. Optically-stimulated luminescence and terrestrial cosmogenic nuclide sample locations are shown with "BJ" and "BJC" notations, respectively. Detailed topography generated from total station mapping. Qu is upper surface and Qt designations represent strath terrace surfaces with Qt1 being the highest in elevation. Contour interval is 1 m. Contours are relative to the elevation of control point at dot labeled CP, which is at an elevation of 9.6 m above mean sea level. Arrow shows direction of photo taken in Fig. 5 at arm of terrace surfaces shown by the dashed gray line, which is approximate location of elevation profile in Fig. 7. Color version of this figure in the online version of the paper.

imbricated gravel. The contact between the capping gravels and the fluvial–deltaic red bed deposits below is sharp and commonly displays angular discordance; Fig. 8 shows that the underlying red bed deposits dip ~15° west (left in photo) and that the capping gravels dip ~2° to the east with sharp angular discordance of 15–17°. This angular discordance suggests that erosion occurred after deposition of the red beds and before deposition of the capping, perhaps associated with uplift and tilting of the red beds. The gravels generally consist of pinkish gray, poorly sorted cobbles (Figs. 8 and 9b). The cobbles are sub-angular and consist mostly of <10 cm (but some to 25 cm) granitic (~80%), schistose (<20%), and minor marble, quartzite, and vein quartz components; these cobbles appear to be derived from the local bedrock. Cobble layers are locally separated by lenses of fine- to coarse-grained, poorly sorted, angular sand.

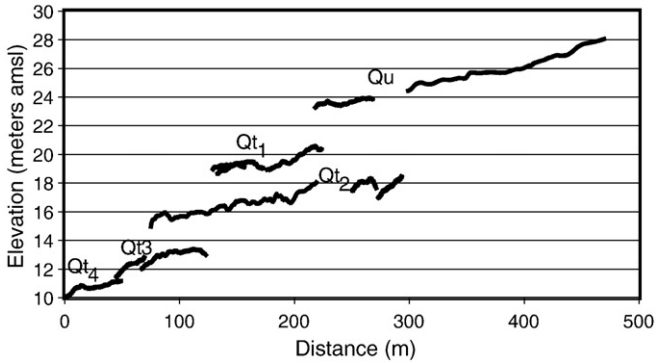

Fig. 7. Elevation versus distance plot. Elevations extracted from the topographic map along terrace spur approximately following the gray dashed line on Fig. 6. Some inset surfaces are preserved up the sides of the spurs and thus two or more terraces are shown at the same distance from the end of the terrace spur (e.g., Qt1 overlaps Qt2). Qu is upper surface. Qt1–Qt4 are inset terrace surfaces.

The surface treads formed on top of the gravels of the upper surface and all the terrace surfaces are similar in composition and morphology; they form a very flat desert pavement that displays subdued to no bar and swale topography. The surfaces are generally made up of similar size (~2–5 cm) clasts of highly weathered granitic material, with tafoni weathering and grus, and with lesser amounts of size-variant and less weathered schist, quartzite, and vein quartz derived from local bedrock. Quartzite and schistose cobbles on the surface display prominent desert varnish but the granitic material is too highly weathered to show varnish.

Soil pits were dug 1.5–2 m in from natural surface edges in the capping gravels of the upper surface (Qu) and lowest terrace tread (Qt4). Soil development in the Qu and the Qt4 deposits extend to depths of at least 75 cm and are very similar in their field characteristics. Av horizons consist of loamy sand and vary between 0 and 4 cm thick. Bk horizons extend from 4 to >75 cm and consist of loamy sand with dry color of 7.5YR5/3. Calcium carbonate coatings <1 mm thick make up ~50% coverage on the bases of clasts, suggesting a stage I+ carbonate morphology (Gile et al., 1981; Machette, 1985; Birkeland, 1999). The similar surface morphology and degree of soil development suggest that the upper surface tread and lowest terrace tread, and therefore the intermediate terrace treads, are similar in age.

7. Optically stimulated luminescence ages

The optically stimulated luminescence dating technique relies on the interaction of ionizing radiation with electrons within semi-conducting minerals (such as quartz) resulting in the accumulation of charge in metastable locations; illuminating the minerals and detrapping the charge causes luminescence (Forman et al., 2000). The luminescence then is used as a proxy for radiation dose, termed equivalent dose (D_E), experienced by the grains since burial. The OSL age can be computed from D_E and an estimate of the environmental

Fig. 8. Photograph showing fluvial–deltaic deposits overlain by capping gravels to form the upper surface. Location A is collection site for sample BJ2 and cosmogenic age profile for upper surface. Location B is sample site for sample BJ3, which was collected from the fluvial–deltaic deposits about 35 cm under the capping gravels. Dashed white line shows approximate bedding orientation in fluvial–deltaic deposits. Note the angular discordance of 15–17° between gravels and fluvial–deltaic deposits. View is to the northwest. Person is 2 m high for scale.

dose rate derived from measured concentrations of radioisotopes (Age = D_E/dose rate). The uncertainty in the age is influenced by the systematic and random errors in the D_E values and the possible temporal changes in the radiation flux. The quoted error is the result of the variation of the D_E values on multiple sub-samples and the error in measured dose rate. It is not possible to determine temporal changes in the dose rate resulting from changes in water content and the growth and/or translocation of minerals within the sediment. The dose rate is therefore assumed to have remained constant over time.

7.1. OSL sampling, preparation, and dating details

Eight samples were collected by hammering opaque plastic tubes into walls of pits dug >1 m from the surface edges into the capping gravel and underlying fluvial–deltaic deposits. The tubes were sealed at their ends and stored in a light-tight sample bags to ensure minimal light exposure. Sub-samples were collected to provide material to measure moisture content and for instrumental neutron activation analysis. The samples remained sealed until opened in the laboratory.

In the capping gravels we sampled 5–10 cm-thick, poorly-sorted, fine to pebbly sand intervals that are underlain and overlain by gravel layers (Fig. 9). The sand intervals display primary bedding structures such as laminations and they do not exhibit secondary depositional features such as burrows, which may result in resetting of the luminescence signal. In the fluvial–deltaic red beds, we sampled poorly-indurated, well-sorted, fine-grained sand.

In the laboratory, all the preparation techniques were carried out under safelights to avoid sample bleaching. About 2 cm of material from the ends of the sampling tubes was discarded. Remaining material was dry sieved to obtain a 90–125 μm particle size fraction. Carbonates and organic matter were removed using 10% HCl and 30% H_2O_2, respectively. Sodium polytungstate solutions of different densities and a centrifuge were used to separate the quartz- and feldspar-rich fractions from the heavy minerals. The separated quartz-rich fractions were treated with 49% HF for 80 min to help dissolve any plagioclase feldspars not separated during the heavy liquid treatment and remove the alpha-irradiated surface of the quartz grains. Dried quartz grains were mounted on stainless steel discs with silicon spray.

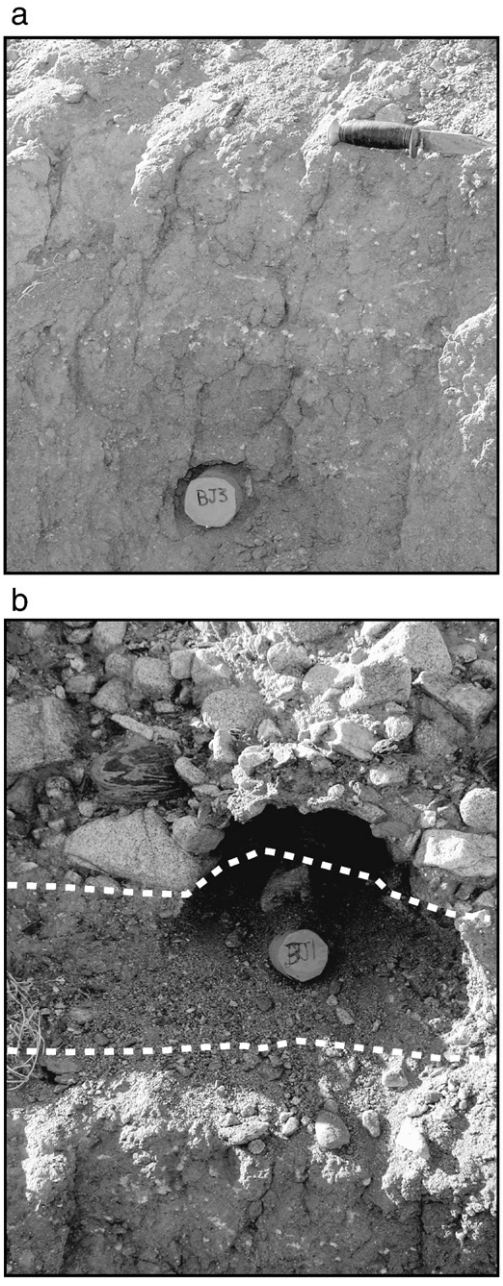

Fig. 9. Field photographs showing representative sections and sample locations of (a) fluvial–deltaic redbeds and (b) the capping gravels. In a, the knife is 20 cm long and marks to location of the unconformity between the capping gravels and the fluvial–deltaic deposits. In b, the white dashed lines show locations of contacts of ~10 cm thick coarse-grained sand layer (sample location) between conglomeratic gravels.

The in situ water content was determined on sub-samples by drying them in an oven at 50 °C.

Luminescence determinations were made on quartz using the single-aliquot regenerative-dose (SAR) protocol of Murray and Wintle (2000) and Banerjee et al. (2001). At least ten D_E measurements were made for each sample. A Daybreak 1100 automated system with an 1100FO/L combined fiber-optic/IRLED illuminator for optical stimulation (Bortolot, 1997) was used for luminescence measurement. Luminescence was stimulated using a 150 W halogen lamp producing green light (514Δ34 nm; ~20 mW cm^{-2}) defined by an additional narrow band interference filter. All quartz samples were screened for feldspar contamination using infrared stimulation from 880Δ80 nm emitting diodes. All OSL signals were detected with a photomultiplier tube characterized by 9 mm Schott UG11 ultraviolet detection filters. Growth curves were plotted using the net natural and regenerated data divided by the subsequent response to the net-test dose. The growth curve data were fitted with either a single saturating exponential or linear function. Two rejection criteria were utilized; if recuperation of the natural level and if the miss-match between repeat regenerative levels was >10%. If a disc failed to meet these criteria the result was discarded and a new disc measured. Successful D_E results for each sample were used to calculate the age of each sample.

Approximately 20 g of the dried sub-sample from each sediment sample was ground to a fine powder and sent to the Becquerel Laboratories at Lucas Heights in Australia for neutron activation analysis to determine U, Th, Rb and K concentrations. These concentrations were converted to external beta and gamma components using the dose-rate conversion factors of Adamiec and Aitken (1998) and beta attenuation factors of Mejdahl (1979) (Table 1). An uncertainty of ±5% water content is applied to help account for possible temporal changes in water content. The methods of Prescott and Hutton (1994), which incorporate a cosmic ray component, were used to estimate the total dose rate for each sample (Table 1).

7.2. OSL results

We collected five OSL samples from the capping gravels of the upper surface and inset terraces and three samples from the red bed fluvial–deltaic deposits below the capping gravels (Table 1). The capping gravels were dated to give age of alluvial fan deposition and, therefore, the ages of the upper surface and the terrace treads. The red bed fluvial–deltaic deposits were dated to give age of these deposits to evaluate time lag between fluvial–deltaic deposition and alluvial fan deposition and also to help constrain range-front uplift magnitude and rate. Fig. 9a shows the location of one sample collected from a sand layer between clay and silt layers in the fluvial–deltaic deposits about 35 cm below the base of the capping gravels. Fig. 9b shows representative sample location from the capping gravel deposits within an approximately 10 cm-thick sand layer surrounded by subangular gravel above and fluvial–deltaic deposits.

Equivalent dose values for individual samples display considerable scatter, with standard deviations of 12 to 32% (Fig. 10). The spread in D_E values probably represents variations in bleaching of samples prior to or during deposition in a fluvial and debris flow depositional setting. However, standard errors of the mean at one standard deviation level are 3 to 7%, indicating a relatively well-constrained mean value for D_E. Dose rate values range from 3.3 to 4.1 Gy/ka (Table 1). Two sand samples from the upper surface (Qu) capping gravels are 16.9 ± 1.5 and 20.1 ± 2.0 ka. One sample from the highest inset terrace (Qt1) is 29.0 ± 2.6 ka. Two samples from the same sand layer in the lowest inset terrace (Qt4) yield OSL ages of 20.9 ± 2.2 and 30.9 ± 2.8 ka. In summary, OSL ages for samples from the capping gravels of the upper surface and terraces range from about 17 to 31 ka (Fig. 10), with a pooled average age of 24 ± 3 ka (standard error of the mean).

OSL ages from the capping gravels lack a systematic change from the upper surface to lowest terrace (Qt4) surfaces. One might expect to see a younging of ages with decreasing surface height because younger terrace surfaces get incised (at lower elevations) into older ones. Additionally, repeat ages from the same sand layer in Qt4 show an age range that is comparable to the age range across all the surfaces. This age variation probably reflects the true uncertainty in OSL ages for any of the surfaces at this location. The lack of systematic change in OSL age with surface height, as well as the similarity in surface morphology and composition, suggests that the upper surface and terrace capping gravels formed in a relatively short time span shown by the age range of 17 to 31 ka. Additionally, some of the OSL age variation may be related to reworking of capping gravel sediments and ineffective charge zeroing during deposition.

The samples from the fluvial deltaic red bed deposits (samples BJ3, BJ06-1, BJ06-2) all have OSL ages that are older than those from the capping gravels (Table 1; Fig. 10). The OSL ages for these samples range from 31.1 ± 2.1 to 37.9 ± 4.2 ka. This age range is younger than 40–60 ka U-series ages of Carter (1977) from a paleosol in similar deposits farther south at the south end of the Sierra El Mayor. Carter (1977) interpreted the paleosol ages as minimum ages and suggested that these Colorado River fluvial–deltaic deposits were related to deposition during the Sangamonian (~120 ka) sea-level highstand.

Table 1
Optically stimulated luminescence age data.

Sample #/ Lab ID	Sediment type[a]	K (%)[b]	Rb (ppm)[b]	Th (ppm)[b]	U (ppm)[b]	Water content (%)[c]	Cosmic dose rate (Gy/ka)[d]	Total dose rate (Gy/ka)[e]	D_E (Gy)[f]	n[g]	Age (ka)
Capping gravels											
BJ2	CGQ-A	2.62	93.2	7.73	1.79	0.1	0.18 ± 0.02	3.68 ± 0.26	62.2 ± 1.7	19	16.9 ± 1.5
BJ4	CGQ-B	2.09	88.7	8.00	2.41	0.5	0.20 ± 0.02	3.35 ± 0.22	67.4 ± 4.0	17	20.1 ± 2.0
BJ5	CGQ-B	3.02	99.1	7.47	1.94	0.4	0.19 ± 0.02	4.08 ± 0.29	85.3 ± 5.0	10	20.9 ± 2.2
BJ7	CGQ-B	2.21	93.5	8.62	2.18	0.5	0.20 ± 0.02	3.45 ± 0.23	100.0 ± 3.3	18	29.0 ± 2.6
BJ8	CGQ-A	2.05	91.8	9.48	2.53	1.7	0.19 ± 0.02	3.40 ± 0.22	105.0 ± 4.3	26	30.9 ± 2.8
Fluvial–deltaic red-bed deposits below capping gravels											
BJ3	CGQ-A	2.17	86.4	7.12	2.26	0.6	0.17 ± 0.02	3.30 ± 0.22	125.2 ± 9.3	18	37.9 ± 4.2
BJ06-1	CGQ-A	1.85	87.3	8.95	3.20	0.6	0.19 ± 0.02	3.22 ± 0.22	103.4 ± 1.9	20	32.1 ± 2.1
BJ06-2	CGQ-A	1.73	70.5	6.82	2.14	0.6	0.18 ± 0.02	2.70 ± 0.17	84.0 ± 1.8	20	31.1 ± 2.1

[a] Analysis for coarse-grained (90–125 mm) quartz fraction (CGQ) on (A) poorly sorted sand and (B) pebbly sand.
[b] Uncertainties on analyses of U, Th, Rb and K are taken to be ±10%.
[c] Uncertainty taken as ±5%.
[d] Cosmic doses and attenuation with depth were calculated using the methods of Prescott and Stephan (1982) and Prescott and Hutton (1994).
[e] Total doses combine the cosmic dose rate and the beta and gamma doses calculated from the K, Rb, Th and U concentrations in the sediment using the methods of Adamiec and Aitken (1998) and Mejdahl (1979) with corrections for moisture content after Zimmerman (1971).
[f] Average equivalent dose (D_E) and standard error ($1\sigma_{n-1}/n^{1/2}$ of the D_E), incorporating the error from beta source estimated at about ±5%.
[g] Number of equivalent dose values. Each D_E has repeat regenerative levels with less than 10% mismatch (see text).

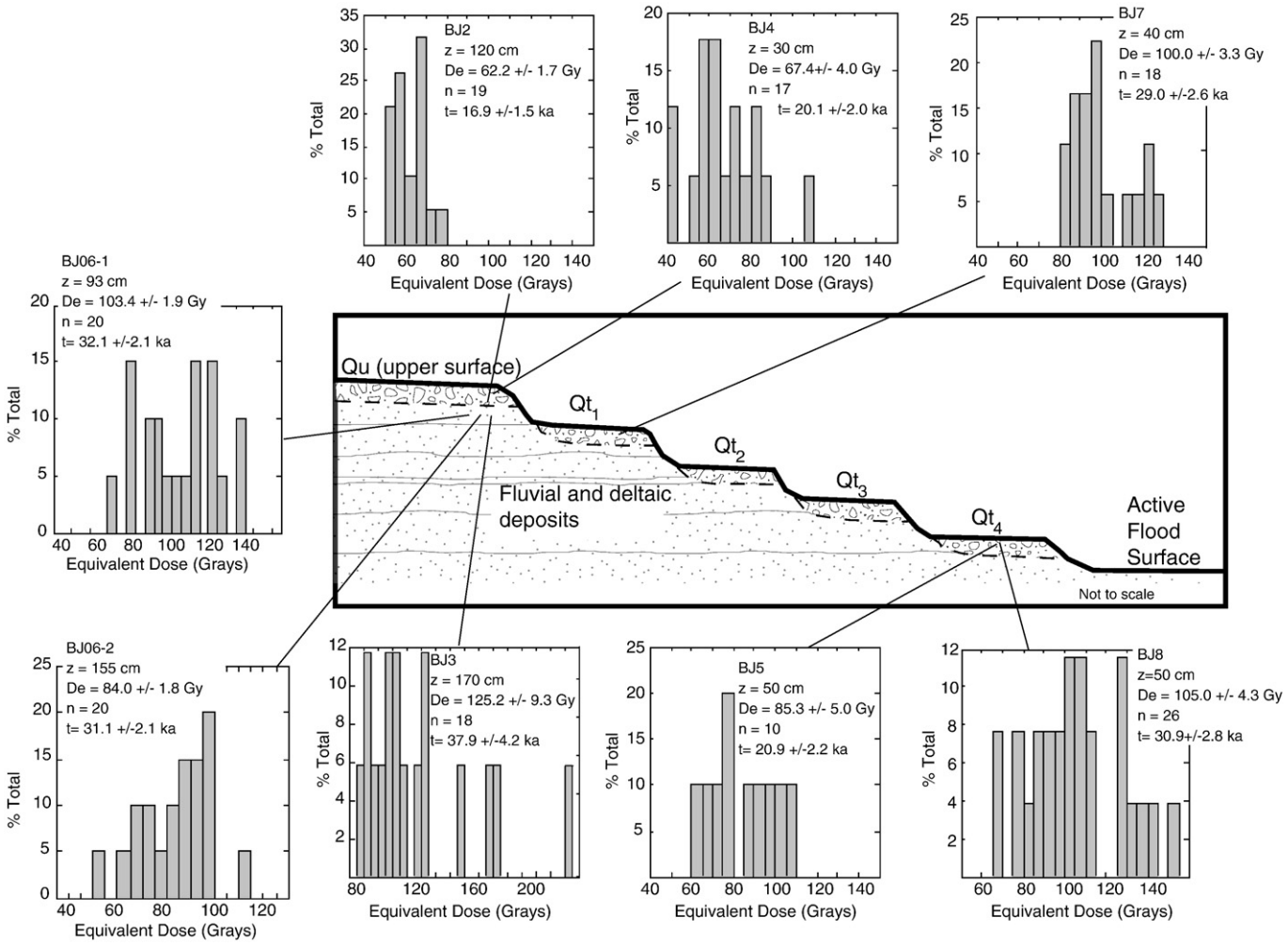

Fig. 10. Optically-stimulated luminescence data shown relative to generalized terrace surfaces. Each histogram plot shows distribution of equivalent dose (D_E) values. BJ# is sample number, z is depth below surface, n is number of successful D_E measurements (see text) used to determine mean D_E, and t is OSL age. The uncertainties are standard error of the mean (at 1σ).

Our new age for the fluvial–deltaic deposits is somewhat less than the youngest age of Carter (1977) and is similar to the lower age range of 35–70 ka for the Chemehuevi beds near Lake Mohave (House et al., 2005) and 32–60 ka aggradation units that are cut by terraces farther up the Colorado River near Yuma (Lundstrom et al., 2004). Thus, aggradation and delta deposition at this time seems to have been prevalent from the delta to near the mouth of the Grand Canyon during Marine Isotope Stage 3 (MIS-3). The fluvial–deltaic deposits directly under the Sierra El Mayor upper alluvial surface do not appear to be related to the Sangamonian highstand, but probably formed during MIS-3 when sea level was ~60–80 m lower than present (e.g., Chappell et al., 1996; Lambeck and Chappell, 2001; Cutler et al., 2003).

8. Terrestrial cosmogenic nuclide ages

Terrestrial in situ cosmogenic surface exposure dating allows a determination of the duration that a rock and/or sediment surface has been exposed to cosmic rays resulting in the production of terrestrial cosmogenic nuclides such as ^{10}Be and ^{26}Al by spallation (Gosse and Phillips, 2001). Measuring the concentrations of ^{10}Be within rock surfaces or sediments allows the age of exposure to be defined.

8.1. Terrestrial cosmogenic nuclide sampling, preparation, and dating details

To attempt to fully assess the exposure ages of the upper surface and terraces, terrestrial cosmogenic nuclide (TCN) ages were obtained: (1) on depth profiles in the alluvial sediments from the upper surface and the lowest terrace; (2) from surficial samples on the upper surface; and (3) on clasts from modern drainages and hillslopes. Assuming the fluvial or alluvial clasts were deposited over a time period that is short relative to deposit age, depth profiles can be used to assess nuclide inheritance and the age of the deposit (Anderson et al., 1996; Repka et al., 1997). Samples from modern drainages and from active hillslopes provide additional constraints on TCN age inheritance because these samples would either have just been deposited (drainages) or are still in place before being deposited (hillslopes).

We collected capping gravel depth profiles from the upper surface (Qu) and the lowest terrace (Qt4) for TCN dating. Pits were dug 1–2 m laterally into the terrace to ensure results were not affected by lateral erosion effects. Approximately 1 kg of random sand and angular gravel (2–4 cm) samples were collected at a spacing of 20 cm to depth of 100 cm. Two surface samples were collected from on top of the upper surface. Sample BJC6 is an ~20×25 cm angular piece of quartzite with a varnished joint or fracture surface facing up (Fig. 11). Sample BJC7 consists of approximately 20 random clasts of 5 cm angular vein quartz from the upper surface.

To assess ^{10}Be inheritance in our depth profile and surface TCN samples, we collected samples from active drainages and a hillside scree slope. Two of the drainage samples (BJC14, BJC15) were collected from small drainages between spurs of the surfaces (Fig. 6). The dominant sources of the alluvial material in these drainages are the upper and inset terrace surfaces; presumably if a new terrace was formed with the

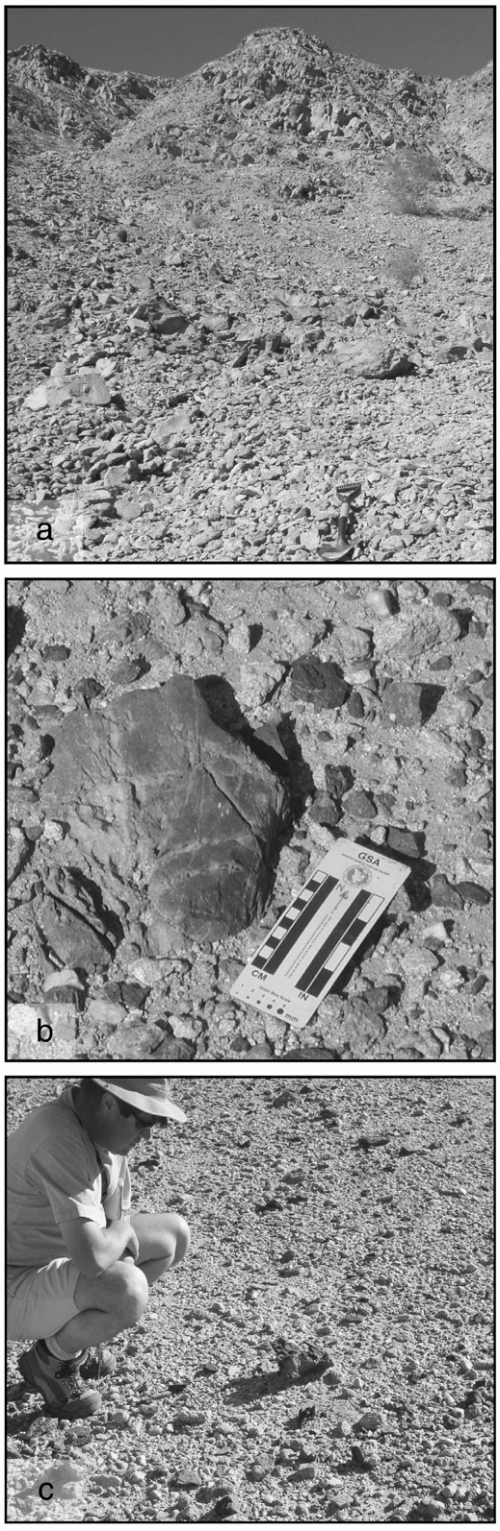

Fig. 11. Field photographs showing cosmogenic age surface sampling locations. (a) View shows scree slope sampled for sample BJC17. This slope is a typical granitic slope adjacent to the upper surface. Shovel at bottom of photograph is 1 m long. (b) Photograph shows undisturbed quartzite cobble collected for sample BJC6. (c) Typical view of the upper surface sampled for BJC7 random vein quartz clasts.

present drainage gravels capping the terrace, then the inheritance would be equivalent to the ^{10}Be concentration in the modern alluvial materials. Our sampling approach allows us to test potential inheritance in the capping gravels at the time of their formation. We collected one additional sample (BJC16) from a major drainage that samples detritus from a drainage basin in the range. This sample should integrate the possible effects of material that is farther traveled than the material derived from the terraces themselves. In all drainage samples, approximately 2–3 kg of 2–5 cm random clasts and coarse sands were collected. Sample BJC17 was collected from an active scree slope at the base of a steep granitic slope (Fig. 11) adjacent to the upper surface and consisted of 5–10 cm angular granitic clasts. This sample tests the potential inheritance that might occur as the source material is being eroded and before transport to the surfaces.

The samples were crushed and sieved. Quartz was then separated from the 250–500 μm size fraction using the method of Kohl and Nishiizumi (1992). After addition of Be carrier, Be was separated and purified by ion-exchange chromatography and precipitation at pH > 7. The hydroxides were oxidized by ignition in quartz crucibles. BeO were mixed with Nb metal and loaded onto targets for ^{10}Be/^{9}Be determination by accelerator mass spectrometry at the Center for Accelerator Mass Spectrometry in the Lawrence Livermore National Laboratory. Isotope ratios were compared to ICN ^{10}Be standards using a ^{10}Be half-life of 1.5×10^6 yr.

The measured isotope ratios were converted to TCN concentrations in quartz using the total Be in the samples and the sample weights. Radionuclide concentrations were then converted to zero-erosion exposure ages using the scaling method of Stone (2000) and were corrected for geomagnetic field variations as described in Farber et al. (2005).

8.2. TCN results

Table 2 and Fig. 12 summarize ^{10}Be and computed age results for the depth profile, surface top, drainage, and scree slope samples. Both capping gravel depth profiles lack a systematic decrease in ^{10}Be concentration with increasing depth (Table 2). The lack of a decrease in ^{10}Be with depth suggests that these samples have retained considerable inheritance that overwhelms the effects of cosmic ray penetration in our samples. Additionally, arid zone fan sediments will have complex exposure/burial histories both in catchment and on the fan itself, subject to extreme variability and complexity in terms of sediment generation, transport, deposition, and re-working due to the low frequency–high magnitude nature of storm and flood events. Corrected TCN ages in the capping gravel depth profile of the upper surface range from 45 to 73 ka (Fig. 12). The pooled (mean) age for the pediment depth profile is 57 ± 4 ka (at 1 standard error, $n = 5$). In the capping gravel depth profile for Qt4, the ages range from 40 to 104 ka. However, sample BJC10 ^{10}Be age is a clear outlier relative to the other samples and has a ^{10}Be concentration that is 170% higher than the average of the other four samples. Thus, we omit BJC10 and use the other four ages in the depth profile to compute a pooled age of 62 ± 11 ka for the Qt4 terrace capping gravels.

The two surface samples from the upper surface yield TCN ages of 47 and 66 ka with a mean age of 56 ± 10 ka. Assuming that pre-depositional inheritance is random at one location, and noting that the pooled ages of the depth profiles and the surface samples from different locations overlap within uncertainty levels, we pool the depth profile and surface sample ages to compute a TCN age that accounts for the observed age variation. This pooled age is 59 ± 5 ka for all the samples.

The drainage and scree slope samples are considerably younger than almost all the depth profile and pediment/terrace surface samples. The samples from the two terrace-sourced drainages yield TCN ages of 44 ± 2 and 44 ± 1 ka. The sample from the major drainage yields an age of 26 ± 1 ka, and the scree slope sample yields an age of 37 ± 1 ka. The younger age from the sample from the major drainage is probably due to the more rapid geomorphic processes, such as erosion and deposition rate, caused by greater water collection in the large catchments relative to those in the smaller internal catchments. The pooled TCN age for these four samples is 38 ± 4 ka. This age is

Table 2
Terrestrial cosmogenic nuclide age data.

Sample number	Site type	Depth (cm)	Latitude (°N)	Longitude (°W)	Elev. (m)	^{10}Be (atoms/gm)	Depth corr.[a]	Be age[b] (yrs)	Corr. Be age[c] (yrs)	Aver. age[d] (yrs)
BJC1	Upper surface profile	20	32.142	115.289	25	200,789 ± 18,072	0.85	49,268 ± 4434	45,493 ± 4095	
BJC2	Upper surface profile	40	32.142	115.289	25	187,406 ± 18,110	0.73	51,715 ± 4998	47,761 ± 4615	57204 ± 5396
BJC3	Upper surface profile	60	32.142	115.289	25	185,175 ± 19,358	0.63	57,150 ± 5974	53,207 ± 5562	
BJC4	Upper surface profile	80	32.142	115.289	25	206,399 ± 18,817	0.55	70,974 ± 6471	66,318 ± 6046	
BJC5	Upper surface profile	100	32.142	115.289	25	206,226 ± 20,980	0.48	78,468 ± 7983	73,240 ± 7451	
BJC6	Upper surface	1	32.142	115.289	25	229,194 ± 19,155	0.99	50,388 ± 4211	46,517 ± 3888	56452 ± 9934
BJC7	Upper surface	1	32.142	115.289	25	321,648 ± 18,480	0.99	71,049 ± 4082	66,386 ± 3814	
BJC8	Qt4 profile	20	32.141	115.293	11	171,552 ± 10,396	0.85	43,129 ± 2614	40,200 ± 2436	
BJC9	Qt4 profile	40	32.141	115.293	11	206,541 ± 11,279	0.73	58,570 ± 3198	54,700 ± 2987	
BJC10	Qt4 profile	60	32.141	115.293	11	352,154 ± 17,121	0.63	112,947 ± 5491	104,386 ± 5075	62390 ± 10669
BJC11	Qt4 profile	80	32.141	115.293	11	193,112 ± 11,872	0.55	68,085 ± 4186	63,765 ± 3920	
BJC12	Qt4 profile	100	32.141	115.293	11	248,266 ± 12,783	0.48	97,341 ± 5012	90,895 ± 4680	
BJC14	contemporary wash	1	32.141	115.293	10	209,464 ± 8533	0.99	47,214 ± 1923	43,698 ± 1780	
BJC15	contemporary wash	1	32.141	115.293	10	210,685 ± 5688	0.99	47,490 ± 1282	43,943 ± 1186	37721 ± 4153
BJC16	contemporary wash	1	32.141	115.293	10	120,925 ± 4449	0.99	27,131 ± 998	26,228 ± 965	
BJC17	scree slope	1	32.141	115.293	30	174,835 ± 5398	0.99	39,335 ± 1214	37,018 ± 1143	

[a] Depth correction factor using a sediment density of 2.0 g/cm^3.
[b] Ages calculated using Stone (2000) latitude and altitude scaling factors. Sea level high latitude production rate of 5.44 ^{10}Be atoms/g quartz per year. Zero erosion rate.
[c] Includes correction factor for variations of the magnetic field intensity and pole positions.
[d] Average age of the samples for the depth profile or sample set. For the Qt_4 depth profile, sample BJC10 was omitted because of its high ^{10}Be content relative to the other samples in the profile. The errors are one standard error of the mean at one standard deviation level.

interpreted as the average prepositional inheritance age for the capping gravel and surface samples.

Given that the pooled TCN age of 59 ka almost certainly represents both inheritance and time since deposition and that the 38 ka age from the drainages and scree slope represents inheritance age, we compute an average deposition age of 21 ka (59 minus 38 ka) for the capping gravels and surfaces. The uncertainty in the computed deposition ages is considerable. However, assuming a 20% uncertainty, which is about the maximum relative standard error (at 1s.d.) of the pooled depth profile and surface samples, the age span for the TCN-derived deposition age is ca. 16 to 25 ka. This age span is consistent with the depositional age span of 17 to 31 ka from the OSL samples (Table 1).

It is important to note that the inherited ^{10}Be of our samples comprises about half of the total ^{10}Be ages and is the dominating control on fan age. As noted by Gosse (2003), large inheritance is common in the dating of arid region alluvial fans, but its effects diminish with increasing fan age. We have confidence in our inheritance-corrected ages because we were able to positively correlate the TCN ages with OSL ages. Although there is considerable scatter in the OSL and TCN ages, we interpret the ages to represent the age of deposition of the gravels and formation of the surfaces and the scatter in the ages to represent a more realistic uncertainty than any one sample's analytic uncertainty. Spelz et al. (2008) acquired TCN ages for surfaces on the western side of the Sierra El Mayor. They assume zero inheritance in their analysis and compute an average age of 15.5 ± 2.2 ka for one of the main terraces. Even though one might expect similar inheritance issues on either side of the range, the amount of inheritance in their study must be much smaller than on the eastern side of the range because the average ages are smaller. This discrepancy is probably related to the sampling in the two studies. Whereas we sampled small (2–5 cm) clasts for bulk ^{10}Be determination, Spelz et al. (2008) sampled 60 to 90 cm boulders. The smaller cobbles sampled in our study would presumably have spent more time on the hillslopes breaking down from boulder size, whereas the large boulders sampled by Spelz et al. (2008) may have moved down from adjacent hillslopes and farther up drainages in large mass-movement/landslide events during major storms and would have been exposed for far less amounts of time prior to deposition. This inference implies that mass-movement events capable of washing large boulders down drainages during major storms would have occurred at periods that are much less than the ~10^4–10^5 timescales shown by the TCN ages. Frankel et al. (2007) note similar sample size issues in their age dispersion for the Q2c surface in northern Death Valley. The age dispersion in the samples from the youngest dated surface of Spelz et al. (2008) is 11.1 to 26.1 ka; this age range may reflect variations in inheritance from boulder to boulder.

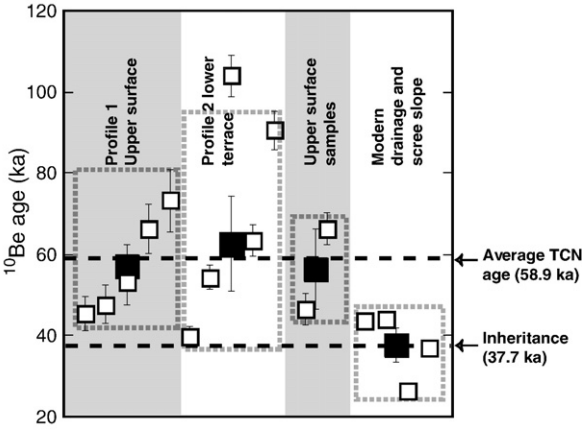

Fig. 12. Plot of ^{10}Be TCN ages for (1) the upper surface depth profile, (2) the lower terrace depth profile, (3) surface samples from the upper surface, and (4) samples from the modern drainages and scree slope. Ages are offset for each data set to show groupings of ages. Large black square is the average for each group and error bar are one standard error (at 1s.d.). Average TCN age (58.9 ka) at right is average of the pooled upper surface profile, lower surface profile, and surface samples. Inheritance at right is average of modern drainage and scree slope.

9. Regional correlation of surfaces

Spelz et al. (2008) used TCN methods on boulders to date two of the eight surfaces on the western side of the Sierra El Mayor; their samples yielded exposure ages of 204 ± 11 ka (their Q7 surface) and 15.5 ± 2.2 ka (their Q4 surface). The 15.5 ka age for Q4 on the west side of the Sierra El Mayor is slightly younger than the 17–31 ka age determined for all the surfaces on the east side of the Sierra El Mayor. However, Spelz et al. (2008) show an exposure age range from 11.1 to 26.1 ka for different boulders from their Q4. Surface morphology descriptions are similar for Spelz et al. (2008) Q4 surface and our

surfaces. Thus, the surfaces of this study correlate well in terms of age and physical characteristics with Q4 of Spelz et al. (2008). Mueller and Rockwell (1995) described five alluvial deposits and surfaces along the Laguna Salada fault adjacent to Laguna Salada (Figs. 2 and 3). Soil and morphology descriptions for their Q4 deposit closely match the descriptions of the surfaces in this study. However, Mueller and Rockwell (1995) used regional correlations from soil descriptions in the Imperial Valley area ~50 km to the north to assign an age of 4–8 ka for the alluvial deposits, which is considerably younger than our dated deposits and surfaces. Our new ages for similar deposits and surfaces on the eastern side of the Sierra el Mayor, as well as the ages from Spelz et al. (2008), may place new age constraints on the Q4 deposits of Mueller and Rockwell. Alternatively, the age equivalent deposits to those of our study and those of Spelz et al. (2008) may not have been deposited along the Laguna Salada fault area and an alluvial fan surface intermediate to Mueller and Rockwell's (1995) Q4 and the older Q5 may be missing.

The surfaces of the eastern Sierra El Mayor are located along the modern delta of the Colorado River. Terraces along the Colorado River system downstream of the Grand Canyon are common and have been studied extensively (e.g., Lee, 1908, Blackwelder, 1933, 1934; Longwell, 1936; Metzger and Loeltz, 1973). House et al. (2005) summarize previous work and describe Neogene to Holocene aggradation surfaces and terraces along the Colorado River in the Lake Mohave and Mohave Valley region farther north (Fig. 1). Blackwelder (1933) described 9–12 terraces along the Colorado River in the Yuma area (Fig. 1), which he attributed to climate change or sea level change in the Sea of Cortez. Lundstrom et al. (2004) report ages of about 32 to 60 ka for aggradational sequences that were subsequently cut by terrace flights along the river near Yuma approximately 50 km north of the Sierra el Mayor. They attributed the aggradation and later incision to the yield response of the complex river system to various mechanisms, including climate change. The terraces at Yuma are older than those of the Sierra El Mayor and they would have been less influenced by Sea of Cortez base-level change, and with a longer lag time, than terraces formed along the river closer to the mouth.

A regional chronology for southwestern North America alluvial fan and terrace deposits based on geomorphic expression and soil characteristics is described by Bull (1991, 2007). These include from older to younger Q1, Q2 (a,b,c), Q3 (a, c), and Q4. The Q2c surface is generally considered Late Pleistocene (~60 ka) and the Q3a surface early Holocene (~12 ka). Klinger (2002) also subdivided the Q2 surface into three subdivisions (Q2a, Q2b, and Q2c) for fans in northern Death Valley, with youngest (Q2c) having an age range of ~35–60 ka (Klinger, 2001); the ages for Death Valley fan deposits and surfaces are summarized by Knott et al. (2005) and Sohn et al. (2007). Frankel et al. (2007) describe similar Q2c surfaces in northern Death Valley that have cosmogenic ages of 36 to 82 ka, in about the same age range of that prescribed by Klinger (2001). Sohn et al. (2007) acquired an age of 25 ka from an alluvial fan in southern Death Valley. This age is between the youngest Q2c and the oldest Q3c surfaces and thus Sohn et al. (2007) classified that fan surface as Q2d. Spelz et al. (2008) follow Q2d designation for their Q4 surface. In the regional context, then, the 17–30 ka surfaces that we mapped and dated on the eastern side of the Sierra El Mayor (Qu through Qt4 in our nomenclature) probably correlate with the regional Q2d (between Q2c and Q3a).

10. Discussion

10.1. Formation of the alluvial deposits and surfaces of the eastern Sierra El Mayor

Both OSL and TCN ages indicate that the upper surface (Qu) and terrace tread capping gravels and surfaces formed ca. 17–30 ka. This age is only slightly younger than the 31–38 ka age for the fluvial–deltaic deposits on which the upper surface and terrace treads formed. As outlined by Spelz et al. (2008), there are generally two classes of process–response models for aggradation and degradation during the formation of sand and gravel alluvial sequences (see reviews by Wells et al., 1987; Bull, 1991, 2000; Blum and Tornqvist, 2000). In one end-member model, alluvial fans form during transitions from wet to dry conditions whereby the dry conditions lead to reduced vegetation, reduced infiltration rates, and increased exposure of soil to erosion, which then leads to increased sediment supply and aggradation of alluvial fans (e.g., Wells et al., 1987; Bull, 1991). Deposition of the alluvial material continues until an erosion–deposition threshold is crossed, generally either by increased stream power or decreased sediment supply, and the stream starts to incise through the surface (e.g., Bull, 2007). The other end-member for the formation of aggradation and incised fan sequences points toward the transition from dry to relatively wet conditions during the transition from interglacial/interstadial periods to glacial periods (Harvey et al., 1999a,b). Harvey et al. (1999a) worked on coastal alluvial fans in southeast Spain where glacial periods were overall drier than in southwest North America, but seasonal storms were intense. The storms during glacial periods increased sediment supply and fan aggradation (Harvey et al., 1999a). Harvey et al. (1999b) interpreted alluvial fan aggradation in the Mojave area of southwest North America during the transition from Pleistocene to Holocene to be caused by increased sediment supply during summer storms, which were related to zonal circulation weakening and monsoonal incursion of tropical air from the Gulf of Mexico. In this model, the wetter conditions lead to more erosion and increased deposition and the thresholds that change patterns of aggradation and incision are crossed at a high frequency.

The Sierra El Mayor presently has an arid to hyperarid climate. Though there is no direct evidence of a Late Pleistocene arid climate in the Sierra El Mayor, packrat midden studies in the Puerto Blanco Mountains located about 250 km east of the Sierra el Mayor indicate rainfall amounts in the Late Pleistocene were ~280 mm/yr and slightly greater than present-day amounts of ~230 mm/yr at that location (Van Devender, 1977). These rainfall amounts are ~2–5 times higher than present rainfall amounts in the Sierra El Mayor area and it follows that Late Pleistocene rainfall amounts in the Sierra El Mayor were also lower than those in the Puerto Blanco Mountains. The Late Pleistocene climate in the Sierra El Mayor was probably wetter than today, but still arid (as defined by Bull, 1991) and with similar vegetation cover. Van Devender (1977) shows that even during wetter glacial periods portions of the Mojave Desert region, and probably the Sierra El Mayor, never developed significant vegetation under elevations of 500 m; the lower Colorado River area probably has been an arid desert environment that supported typical Mojave Desert flora for much of the Quaternary (Cole, 1986; Van Devender, 1977). Therefore, it is likely that vegetation coverage was sparse in the low-elevation Colorado River delta area during transition from the Middle Wisconsinan interstadial to the Late Wisconsinan full glacial (MIS-3 to MIS-2 in Fig. 13) and that alluvial fan aggradation was caused by increasing rainfall during the transition to the last full glacial rather than caused by a decrease in vegetation cover. Spelz et al. (2008) also interpret their Q4 surface (15.5 ka) on the western side of the Sierra El Mayor as forming during the transition from drier to wetter conditions during the Late Wisconsinan Substage (MIS-2). Similarly, Hanson (2005) interpreted the ~10–35 ka alluvial fan aggradational sequences farther upstream along the lower Colorado River as responses to the change from drier to wetter conditions. Thus, the overall formation of the eastern Sierra El Mayor alluvial fan aggradation events are interpreted to be related to transition from dry to relatively wet conditions when increased rainfall caused increased erosion and alluvial fan deposition.

Interpretations of the genesis of the terrace straths along the eastern Sierra El Mayor must account for their local nature. The small riser sizes of the terraces (1–2 m) suggests a relatively rapid response

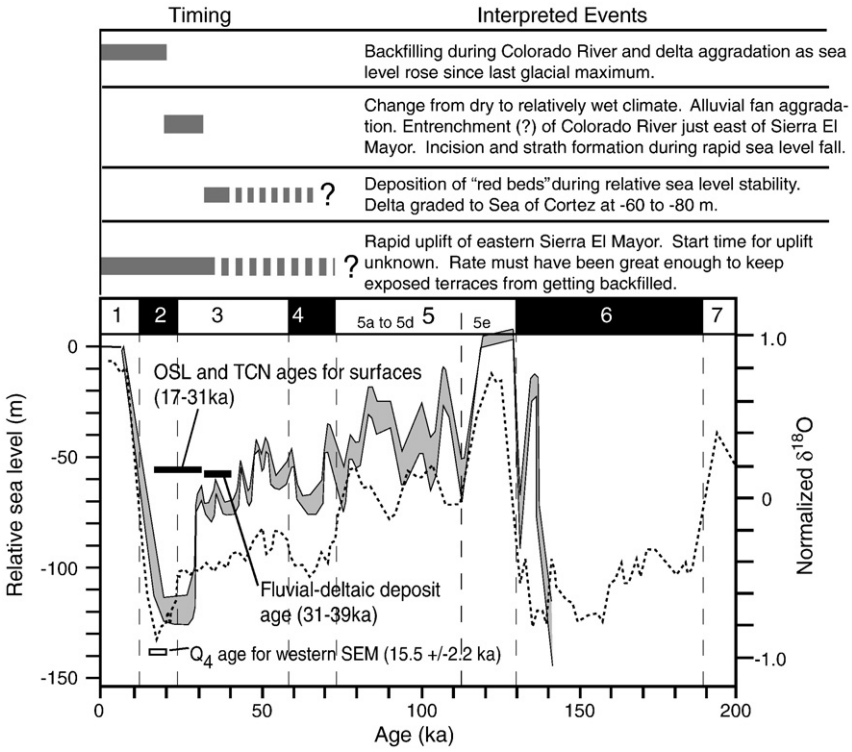

Fig. 13. Relative sea-level curve (gray bracketed region) (from Lambeck and Chappell, 2001) and normalized $\delta^{18}O$ curve (modified from Martinson et al., 1987) showing optically stimulated luminescence (OSL) and ^{10}Be terrestrial cosmogenic nuclide (TCN) age distributions for the eastern Sierra El Mayor (SEM) surfaces and fluvial–deltaic deposits from this study. Also shown is the age of the Q_4 surface from the west side of the Sierra El Mayor (Spelz et al., 2008). Numbers 1–7 are Marine Isotope Stages. Note that the fluvial–deltaic deposits were deposited during relative stability of Marine Isotope Stage 3 and the surfaces formed during Marine Isotope Stage 2 when there was an abrupt drop in $\delta^{18}O$ and associated glaciation and sea-level fall. Chart at top shows relative timing of interpreted events discussed in text.

time at relatively close distances to the local base level. During the change from interstadial to the full glacial (MIS-3 to MIS-2), sea level was falling rapidly from ca. −70 to −80 m at 30–35 ka to ca. −110 to −130 m at 18 ka (Chappell et al., 1996; Lambeck and Chappell, 2001); these age relations suggest that the abandonment of the upper surface and formation of the inset terraces are linked to the nearby Sea of Cortez lowering and the response of the lowermost Colorado River and its delta to this base-level change. Though a prominent alluvial plain surface at similar elevations is located along other mountain ranges facing the delta farther south, similar terrace flights are not located along these mountain fronts. The alluvial plain surfaces along other ranges have been interpreted as representing aggradation to the Sangamonian high sea level at ~120 ka (Carter, 1977; Ortlieb, 1991). Our interpretation is that the upper surface was stranded and strath terraces cut in response to rapid downcutting through the delta deposits during possible entrenching of the Colorado River just east of the Sierra El Mayor as sea level fell rapidly during the transition from MIS-3 to MIS-2. The local nature of the terraces indicates that the entrenched river must have been close to the Sierra El Mayor. The eastern side of the Sierra El Mayor has a scalloped, concave geometry that faces eastward toward the delta (Figs. 2 and 3). This geomorphic feature possibly formed along an entrenched bend in the Colorado River during the MIS-2. Lowering local base level and increased rainfall would have the net effect of increased stream power during the transition from dry to relatively wet climate in MIS-2 (Fig. 13) and may have allowed the rapid down-cutting and lateral erosion in adjacent drainages and the formation of the terraces on the eastern Sierra El Mayor. The rapid incision of the river, and hence the tributary terrace formation, was probably enhanced by changes in river discharge and yield due to climate change, with time-lagged terrace formation 50 km upstream near Yuma (Blackwelder, 1933; Lundstrom et al., 2004).

Each of the inset terraces has a capping gravel deposit indicating episodic alluviation periods between incision events. This episodic nature may be related to complex response (Bull, 1991) of aggradation–degradation threshold patterns during the overall base-level lowering, perhaps associated with high-frequency climate events and/or individual storm events. However, we cannot rule out the possibility of punctuated surface uplift events during earthquakes that each raised the land surface 1–2 m at the same time sea level was dropping. Mueller and Rockwell (1995) measured 3–4 m of vertical displacement on the most recent event in 1892 on the Laguna Salada fault. If half of this vertical slip is partitioned into footwall uplift and half into hanging wall down-drop, the 1–2 m of surface uplift is reasonable for earthquake events in the Sierra El Mayor fault system. Each of these uplift events would cause an increase in stream power and rapid incision as the local streams re-equilibrate. It is possible that several more terraces associated with this overall terrace-forming event are buried under the delta deposits farther east, but subsequent Holocene sea-level rise and aggradation along the delta caused backfilling of additional terraces. The upper surface and inset terraces of the eastern Sierra El Mayor are preserved because this area has experienced enough uplift and at a high enough rate to strand the terraces above Holocene backfill elevations (see next section).

10.2. Uplift of the Sierra El Major

The Sierra El Mayor–Sierra Cucapá are located at the highly-deformed and active structural transition from the northern Gulf Extensional Province to the San Andreas system (e.g., Siem and Gastil, 1994; Mueller and Rockwell, 1995; Axen and Fletcher, 1998; Axen et al., 1999). Geodetic studies across the Laguna Salada region suggest extension rates of 2–4 mm/yr (Savage et al., 1994). Horizontal extension rates from thermokinematic studies for the last few million years (Axen et al., 2000) and from fault kinematic studies on Quaternary faults on the western side of the Sierra El Mayor (Axen et al., 1999) can account for only about 40% or less of the geodetically

determined 2–4 mm/y extension rate (Savage et al., 1994) across the Laguna Salada–Sierra El Mayor area. These fault studies related to the Sierra El Mayor–Sierra Cucapá have focused mainly on the normal and oblique-slip active faults of the Laguna Salada, Cañon Rojo, and Cañada David detachment fault systems on the western side of the mountain range along the Laguna Salada Basin (Fig. 2) (Mueller and Rockwell, 1995; Axen et al., 1999; Spelz et al., 2008; Fletcher and Spelz, 2009). Mueller and Rockwell (1995) studied faulted alluvial fans along the Laguna Salada Fault and estimated minimum vertical slip rates of 1.9 ± 0.4 mm/yr. Mueller and Rockwell (1995) concluded that the fault has been active in the Holocene and may have last ruptured in 1892. Dorsey and Martin-Barajas (1999) used detailed mapping and stratigraphic analysis to estimate slip rates of 2–4 mm/yr since the Middle Pleistocene in the Sierra El Mayor–Sierra Cucapá region; this slip rate partitions into about 1–2 mm/yr horizontal extension or vertical motion for a 45° dipping fault. Scarps along the west-central Sierra El Mayor were studied by Axen et al. (2000) who concluded that the western Sierra El Mayor area is bound by the Cañada David fault, which is an active low-angle detachment fault with an extension rate of about 1 mm/yr. Thus, the Sierra El Mayor–Sierra Cucapá region has experienced considerable Quaternary rapid extension and related uplift, but earlier studies can only account for about half of the geodetically-determined extension and uplift rates.

The age of the top of the red bed fluvial–deltaic deposits provides important constraints on uplift rate for the eastern side of the Sierra El Mayor where exposed faults are lacking. If the top of the fluvial–deltaic deposits are ca. 31–39 ka and were deposited when the delta graded to sea level at that time, then uplift rates can be estimated. The calculations of uplift amounts and rates given below are upper and lower bounds that depend on whether or not the delta top at the time of deposition was similar in elevation to the delta top today, or whether the delta top graded to a lower Sea of Cortez base level. In either case, these estimates provide useful indicators for discussion of regional uplift magnitudes and rates along the eastern Sierra El Mayor. After accounting for ~1 m of capping gravel deposits, the present elevation of the fluvial–deltaic deposits is 13–17 m above the present delta surface in the field area depending on whether the elevation of the top of the fluvial–deltaic deposits is measured at the range front or on spur away from the range front (Fig. 7). Assuming that the delta top elevation was at the same elevation 35 ka as it is today, then a minimum uplift rate for the eastern side of the Sierra El Mayor would be ~0.4 mm/yr (~15 m divided by 35 ka). However, it is more likely that the delta had graded to a lower Sea of Cortez base level during MIS-3. MIS-3 was a relatively stable climate period when sea level was ~60–80 m lower than present day (Chappell et al., 1996; Lambeck and Chappell, 2001) (Fig. 13) between the last interglacial and the start of rapid sea level fall at about 25 ka in MIS-2. It is unknown to what level the delta graded to during the MIS-3, but a maximum would have been about 60–80 m lower than the present delta surface. A maximum uplift rate of 2.1 to 2.7 mm/yr is computed by assuming an uplift amount that is the sum of sea level at 35 ka (-60 to -80 m) and present elevation of the deposits above the active flood plain ($+15$ m). This inferred uplift rate is slightly higher, but similar, to estimates from geologic slip rates of about 2 mm/yr (Mueller and Rockwell, 1995; Dorsey and Martin-Barajas, 1999) as well as geodetic studies (Savage et al., 1994). This rate is also similar to Quaternary subsidence rates for the Laguna Salada (Contreras et al., 2005), which is a rift basin associated with extension across the entire Sierra El Mayor–Laguna Salada system. If footwall uplift magnitude is similar to the hanging-wall subsidence magnitude, then inferred Quaternary uplift rate is 1.6 mm/yr. However, 1.6 mm/yr is probably a minimum if footwall uplift exceeds hanging wall subsidence as in other major extensional systems (e.g., Armstrong et al., 2003).

There are no faults mapped on the eastern side of the Sierra El Mayor that may accommodate uplift of the range and the terraces preserved along its eastern flank. In contrast, two major active range-bounding faults define the western side of the Sierra El Mayor and Sierra Cucapá (Mueller and Rockwell, 1995; Axen et al., 1999, 2000; Spelz et al., 2008). The Laguna Salada fault strikes southeast along the western side of the Sierra Cucapá and across the region between the sierras El Mayor and Cucapá, then continues under the Colorado delta deposits farther southeast (Fig. 2). This fault broke the surface during the 1892 M_w71 earthquake with slip amounts of 2.5 to 5 m (Mueller and Rockwell, 1991, 1995). Near its southern end, the rupture veered from the NW-striking Laguna Salada fault and followed the N-striking Canon Rojo Fault about 2.5 km (Fig. 2). Farther south, a clear surface-breaking fault array continues for about 33 km (Spelz et al., 2008; Fletcher and Spelz, 2009) above the Cañada David detachment fault, which is a low-angle normal fault (Siem and Gastil, 1994; Axen and Fletcher, 1998). The array of faults along the Cañada David detachment fault includes as many as 15 different fault scarps (Spelz et al, 2008; Fletcher and Spelz, 2009). Axen et al. (1999) suggest that these Quaternary faults merge into the Cañada David low-angle normal fault at depth and were active during slip on the low-angle fault in past earthquakes. It is clear that considerable faulting-related Quaternary uplift has occurred on the west side of the Sierra El Mayor even though no Quaternary-aged faults are mapped on the east side.

Evaluation of Landsat imagery shows that the eastern flanks of southernmost Sierra Cucapá and southern half of the Sierra El Mayor are relatively linear (Fig. 3). The region along the eastern range front has been scalloped out by Colorado River erosion and later backfilled by Holocene deposition. Because of the linear range-front segments, and our analysis of the eastern Sierra El Mayor surfaces, we interpret an eastward facing, NNE-striking normal fault system that has been buried by Holocene delta backfilling (Fig. 3). This buried fault system probably shared accommodation of rapid uplift of the Sierra El Mayor and the Sierra Cucapá. Our interpretation is supported by gravity data for the Mexicali Valley that show a steep gravity gradient and north-south-trending Bouguer gravity trough (-40 mGal) located just east of the Sierra El Mayor (Espinoza, 1988; Chavez et al., 1999), which is consistent with a basin-bounding fault along the eastern Sierra El Mayor. An eastern Sierra El Mayor fault also is consistent with a N–S trend of earthquakes that extends from north of the southeast end of the Sierra Cucupa to as far south as the study area in the eastern Sierra El Mayor (Fig. 2). The inferred faults potentially buried under the delta may be southward extension of the Mexicali spreading center that link the dextral slip Cerro Prieto and Imperial faults (Fig. 2).

Geologic data discussed earlier can account for only about 40% or less of the geodetically determined 2–4 mm/y extension rate (Savage et al., 1994) across the Laguna Salada–Sierra El Mayor area. Axen et al. (2000) suggest that other active faults mapped in the area west of the Laguna Salada may accommodate some of the missing extension. However, much of this missing extension can be accounted for by faults buried under the delta system between the eastern Sierra El Mayor and the Cerro Prieto fault (Fig. 2); assuming a 45° fault and 2 mm/yr uplift rate, as much as 2 mm/yr of extension can be accommodated on unmapped faults. Thus, in the absence of exposed faults along the eastern Sierra El Mayor–Sierra Cucapá, the evaluation of the uplifted upper surface and terraces in this study provide important new data on inferring potential fault structures under the modern Colorado River delta system, which provides insight into understanding strain partitioning in the structural transition from northern Gulf Extensional Province to the San Andreas system.

11. Conclusions

The Sierra El Mayor and Sierra Cucapá lie at a key location where (1) the Gulf Extensional Province transitions northward to the San Andreas Fault system and (2) the Colorado River delta is close to its Sea of Cortez base level. The principal Quaternary features of the

eastern Sierra El Mayor are an upper surface and set of relatively small inset terraces that form on top and cut into Colorado River fluvial–deltaic deposits and that we interpret to record the complex interactions of rapid uplift, climate change, and sea-level change. Combined analysis of optically-stimulated luminescence and terrestrial cosmogenic nuclide ^{10}Be ages, which takes into account ^{10}Be inheritance, indicates that the surfaces all formed about 17 to 30 ka when climate was changing from dry to relatively wet and when sea level was dropping rapidly. The fluvial–deltaic deposits just under the upper surface capping gravels are 31–39 ka and probably formed during relative climate and sea level stability during Marine Isotope Stage 3, which is consistent with similar aggradation deposits farther up the delta. If the fluvial–deltaic deposits are MIS-3 in age and the delta graded to the much lower sea level at that time, then uplift rates of about 2.1–2.7 mm/yr are inferred. The terraces along the Sierra El Mayor probably record rapid response to nearby entrenching of the Colorado River just east of the range and are preserved because the high uplift rate outpaced Holocene aggradation of the Colorado River delta after the last glacial maximum. We interpret that this uplift is accommodated on a fault or fault system that is buried beneath the Colorado River delta east of the Sierra El Mayor. The uplift rates from this study are consistent with geologic and geodetic data for the Sierra El Mayor and Sierra Cucapá and account for much of the missing extensional strain across the area.

Acknowledgements

This research was partially supported by a California State University Fullerton Faculty-Student Research/Creative Activity Grant. We thank J. Fletcher and R. Spelz for their discussions in the field about terraces of the Sierra El Mayor and for preprints of their work on the western side of the range. J. Knott provided valuable help with the soil descriptions. We thank P. Gibbard and an anonymous reviewer for their very helpful and insightful reviews.

References

Adamiec, G., Aitken, M., 1998. Dose–rate conversion factors update. Ancient TL 16, 37–50.

Anderson, R.S., Repka, J.L., Dick, G.S., 1996. Explicit treatment of inheritance in dating depositional surfaces using in situ ^{10}Be and ^{26}Al. Geology 24, 47–51.

Armstrong, P.A., Ehlers, T.A., Chapman, D.S., Farley, K.A., Kamp, P.J.J., 2003. Exhumation of the Central Wasatch Mountains, 1: Patterns and timing deduced from low-temperature thermochronometry data. Journal of Geophysical Research 108, 2172. doi:10.1029/2001JB001708.

Axen, G.J., Fletcher, J.M., 1998. Late Miocene–Pleistocene extensional faulting, northern Gulf of California, Mexico and Salton Trough, California. International Geology Review 40, 217–244.

Axen, G.J., Fletcher, J.M., Martin-Barajas, A., 1998. Late Miocene–Pleistocene detachment faulting in the northern Gulf of California and western Salton Trough and its role in evolution of the Pacific–North American plate boundary. In: Behl, R.J. (Ed.), Guidebook to Field Trip #6, 94th Annual Meeting, Cordilleran Section of the Geological Society of America. Department of Geological Sciences, California State University, Long Beach, Long Beach, California. 20 pp.

Axen, G.J., Fletcher, J.M., Cowgill, E., Murphy, M., Kapp, P., MacMillan, I., Ramos-Velazquez, E., Aranda-Gomez, J., 1999. Range-front fault scarps of the Sierra El Mayor, Baja California: formed above an active low-angle normal fault? Geology 27, 247–250.

Axen, G.J., Grove, M., Stockli, D., Lovera, O.M., Rothstein, D.A., Fletcher, J.M., Farley, K., Abbott, P.L., 2000. Thermal evolution of the Monte Blanco dome: low-angle normal faulting during Gulf of California rifting and late Eocene denudation of the eastern Peninsular Ranges. Tectonics 19, 197–212.

Banerjee, D., Murray, A.S., Boetter-Jensen, L., Lang, A., 2001. Equivalent dose estimation using a single aliquot of polymineral fine grains. Radiation Measurements 33, 73–94.

Bennett, R.A., Rodi, W., Reilinger, R.E., 1996. Global positioning system constraints on fault slip rates in southern California and northern Baja, Mexico. Journal of Geophysical Research 101, 21,943–21,960.

Birkeland, P.W., 1999. Soils and Geomorphology. Oxford University Press, New York. 430 pp.

Blackwelder, E., 1933. Terraces along the lower course of the Colorado River. Proceedings of the Geological Society of America 66 [abs.].

Blackwelder, E., 1934. Origin of the Colorado River. Geological Society of America Bulletin 231, 551–566.

Blum, M.D., Tornqvist, T.E., 2000. Fluvial responses to climate and sea-level change: a review and look forward. Sedimentology 47, 2–48.

Bortolot, V.J., 1997. Improved OSL excitation with fiberoptics and focused lamps. Radiation Measurements 27, 101–106.

Bull, W.B., 1991. Geomorphic responses to climatic change. Oxford University Press, New York. 326 pp.

Bull, W.B., 2000. Correlation of fluvial aggradation events to times of global climate change. In: Noller, J.S., Sowers, J.M., Lettis, W.R. (Eds.), Quaternary Geochronology: Methods and Applications. American Geophysical Union, Washington, D.C., pp. 456–464.

Bull, W.B., 2007. Tectonic Geomorphology of Mountains: A New Approach to Paleoseismology. Blackwell Publishing. 328 pp.

Carter, L.D., 1977. Late Quaternary erosional and depositional history of Sierra del Mayor, Baja California, Mexico. Ph.D. Thesis, University of Southern California, Los Angeles, 262 pp.

Chappell, J., Omura, A., Ezat, T., McCulloch, M., Pandolfi, J., Ota, Y., Pillans, B., 1996. Reconciliation of late Quaternary sea-levels derived from coral terraces at Huon Peninsula with deep sea oxygen isotope records. Earth and Planetary Science Letters 141, 227–236.

Chavez, R.E., Lazaro-Mancilla, O., Campos-Enriquez, J.O., Flores-Marquez, E.L., 1999. Basement topography of the Mexicali Valley from spectral and ideal body analysis of gravity data. Journal of South American Earth Sciences 12, 579–587.

Cole, K.L., 1986. The lower Colorado River Valley: a Pleistocene desert. Quaternary Research 25, 392–400.

Contreras, J., Martin-Barajas, A., Herguera, J.C., 2005. Subsidence of the Laguna Salada Basin, northeastern Baja California, Mexico, inferred from Milankovitch climatic changes. Geofisica Internacional 44, 103–111.

Cutler, K.B., Edwards, R.L., Taylor, F.W., Cheng, H., Adkins, J., Gallup, C.D., Cutler, P.M., Burr, G.S., Bloom, A.L., 2003. Rapid sea-level fall and deep-ocean temperature change since the last glacial maximum. Earth and Planetary Science Letters 206, 253–271.

Dorsey, R., Martin-Barajas, A., 1999. Sedimentation and deformation in a Pliocene–Pleistocene transtensional supradetachment basin, Laguna Salada, north-west Mexico. Basin Research 11, 205–221.

Espinoza, C.J., 1988. Analisis e interpretacion preliminar de los mapas de potencial magnetico y gravimetrico del campo geotermico d Cerro Prieto y sus alrededores, B.C., Mexico. Mexican Geophysical Union.

Farber, D.L., Hancock, G.S., Finkel, R.C., Rodbell, D.T., 2005. The age and extent of tropical alpine glaciation in the Cordillera Blanca, Peru. Journal of Quaternary Science 20, 759–776.

Fletcher, J.M., Spelz, R.M., 2009. Patterns of Quaternary deformation associated with an active low-angle normal fault, Laguna Salada, Mexico: evidence of a rolling hinge? Geosphere 5, 385–407.

Forman, S.L., Pierson, J., 2002. Late Pleistocene luminescence chronology of loess deposition in the Missouri and Mississippi River valleys, United States. Paleogeography, Paleoclimatology, Paleoecology 186, 25–46.

Forman, S.L., Pierson, J., Lepper, K., 2000. Luminescence geochronology. In: Noller, J.S., Sowers, J.M., Lettis, W.R. (Eds.), Quaternary Geochronology: Methods and Applications. American Geophysical Union, Washington, D.C., pp. 157–176.

Frankel, K.L., Brantley, K.S., Dolan, J.F., Finkel, R.C., Klinger, R.E., Knott, J.R., Machette, M.N., Owen, L.A., Phillips, F.M., Slate, J.L., Wernicke, B.P., 2007. Cosmogenic ^{10}Be and ^{36}Cl geochronology of offset alluvial fans along the northern Death Valley fault zone: implications for transient strain in the eastern California shear zone. Journal of Geophysical Research 112. doi:10.1029/2006JB004350.

Frez, J., Gonzalez, J.J., 1991. Crustal structure and seismotectonics of northern Baja California. In: Dauphin, J.P., Simoneit, B.T. (Eds.), Gulf and Peninsular Province of the Californias: American Association of Petroleum Geologists Memoir, vol. 47, pp. 261–284.

Gastil, R.G., Phillips, R.P., Allison, E.C., 1975. Reconnaissance Geology of the State of Baja California: Geological Society of America Memoir, vol. 140. 170 pp.

Gile, L.H., Hawley, J.W., Grossman, R.B., 1981. Soils and Geomorphology in the Basin and Range Area of Southern New Mexico: Guidebook to the Desert Project: New Mexico Bureau of Mines and Mineral Resources Memoir, vol. 39. 222 pp.

Gosse, J.C., 2003. Cosmogenic nuclide dating of arid region alluvial fans. Geological Society of America Abstracts with Programs, p. 228.

Gosse, J.C., Phillips, F.M., 2001. Terrestrial in situ cosmogenic nuclides: theory and application. Quaternary Science Reviews 20, 1475–1560.

Hanson, P.R., 2005. Alluvial fan response to climate change along the lower Colorado River. Geological Society of America Abstracts with Programs 37, 110.

Hanson, P.R., Mason, J.A., Goble, R.J., 2004. Episodic late Quaternary slopewash deposition as recorded in colluvial aprons, southeastern Wyoming. Quaternary Science Reviews 23, 1835–1846.

Harvey, A.M., Silva, P.G., Mather, A.E., Goy, J.L., Stokes, M., Zazo, C., 1999a. The impact of Quaternary sea-level and climatic change on coastal alluvial fans in the Cabo de Gata ranges, southeast Spain. Geomorphology 28, 1–22.

Harvey, A.M., Wigand, P.E., Wells, S.G., 1999b. Response of alluvial fan systems to the Late Pleistocene to Holocene climatic transition: contrasts between the margins of pluvial Lakes Lahontan and Mojave, Nevada and California, USA. Catena 36, 255–281.

House, P.K., Pearthree, P.A., Howard, K.A., Bell, J.W., Perkins, M.E., Faulds, J.E., Brock, A.L., 2005. Birth of the Lower Colorado River — stratigraphic and geomorphic evidence for its inception near the conjunction of Nevada, Arizona, and California. In: Pederson, J., Dehler, C.M. (Eds.), Interior Western United States. Geological Society of America, pp. 357–387.

Klinger, R.E., 2001. Stop A3: Evidence for large dextral offset near Red Wall Canyon. In: Machette, M.N., Johnson, M.L., Slate, J.L. (Eds.), Quaternary and Late Pliocene

Geology of the Death Valley Region: Recent Observations on Tectonic, Stratigraphy, and Lake Cycles. U.S. Geological Survey Open File Report 01-51, pp. A32–A37.
Klinger, R.E., 2002. Quaternary stratigraphy and geomorphology of northern Death Valley — Implications for tectonic activity aong the northern Death Valley fault, Ph.D. thesis, University of Colorado, Boulder, 312 pp.
Knott, J.R., Sarna-Wojcicki, A.M., Machette, M.N., Klinger, R.E., 2005. Upper Neogene stratigraphy and tectonics of Death Valley — a review. Earth-Science Reviews 73, 245–270.
Kohl, C.P., Nishiizumi, K., 1992. Chemical isolation of quartz for measurement of in-situ-produced cosmogenic nuclides. Geochimica et Cosmochimica Acta 56, 3583–3587.
Lambeck, K., Chappell, J., 2001. Sea level change through the Last Glacial Maximum. Science 292, 679–686.
Lee, W.T., 1908. Geological reconnaissance of a part of western Arizona. United States Geological Survey Bulletin 252, 41–45.
Lee, J., Spencer, J.Q., Owen, L.A., 2001. Holocene slip rates along the Owens Valley fault, California: implications for the recent evolution of the Eastern California Shear Zone. Geology 29, 819–822.
Longwell, C.R., 1936. Geology of the Boulder Reservoir floor, Arizona–Nevada. Geological Society of America Bulletin 47, 1393–1476.
Lundstrom, S.C., Mahan, S.A., Paces, J.B., Hudson, M.R., 2004. Late Pleistocene aggradation and incision of the lower Colorado River downstream of the Grand Canyon. Geological Society of America Abstracts with Programs 36, 550.
Machette, M.N., 1985. Calcic soils and calcretes of the southwestern United States. In: Weide, P.L. (Ed.), Soils and Quaternary Geology of the Southwestern United States. Geological Society of America Special Paper, vol. 203, pp. 1–21.
Machette, M.N., Personius, S.F., Nelson, A.R., 1992. The Wasatch Fault Zone, USA. Annales Tectonicae 6, 5–39.
Mahan, S.A., Miller, D.M., Menges, C.M., Yount, J.C., 2007. Late Quaternary stratigraphy and luminescence geochronology of the northeastern Mojave Desert. Quaternary International 166, 61–78.
Martin-Barajas, A., Vasquez-Hernandez, S., Carreno, A.L., Helenes, J., Suarez-Vidal, F., Alvarez-Rosales, J., 2001. Late Neogene stratigraphy and tectonic control on facies evolution in the Laguna Salada Basin, northern Baja California, Mexico. Sedimentary Geology 144, 5–35.
Martinson, D.G., Pisias, N.G., Hays, J.D., Imbrie, J., Moore, T.C., Shackleton, N.J., 1987. Age dating and the orbital theory of the ice ages: development of a high-resolution 0 to 300,000-year chronostratigraphy. Quaternary Research 27, 1–29.
Matmon, A., Schwartz, D.P., Finkel, R., Clemmens, S., Hanks, T., 2005. Dating offset fans along the Mojave section of the San Andreas fault using cosmogenic ^{26}Al and ^{10}Be. Geological Society of America Bulletin 117, 795–807. doi:10.1130/B25590.1.
Matmon, A., Nichols, K., Finkel, R., 2006. Isotopic insights into smoothening of abandoned fan surfaces, southern California. Quaternary Research 66, 109–118.
Mejdahl, V., 1979. Thermoluminescence dating: beta attenuation in quartz grains. Archaeometry 21, 61–73.
Metzger, D.G., Loeltz, O.J., 1973. Geohydrology of the Needles area, Arizona, California, and Nevada. U.S. Geological Survey Professional Paper 486-J. 54 pp.
Mueller, K.J., Rockwell, T.K., 1991. Late Quaternary structural evolution of the western margin of the Sierra Cucapa, northern Baja California. In: Dauphin, J.P., Simoneit, B.T. (Eds.), The Gulf and Peninsular Province of the Californias. American Association of Petroleum Geologists Memoir, vol. 47, pp. 249–260.
Mueller, K.J., Rockwell, T.K., 1995. Late Quaternary activity of the Laguna Salada fault in northern Baja California, Mexico. Geological Society of America Bulletin 107, 8–18.
Murray, A.S., Wintle, A.G., 2000. Luminescence dating of quartz using an improved single-aliquot regenerative-dose protocol. Radiation Measurements 32, 57–73.
Ortlieb, L., 1991. Quaternary vertical movements along the coasts of Baja California and Sonora. In: Dauphin, J.P., Simoneit, B.T. (Eds.), The Gulf and Peninsular Province of the Californias. American Association of Petroleum Geologists Memoir, vol. 47, pp. 447–480.
Peel, M.C., Finlayson, B.L., McMahon, T.A., 2007. Updated world map of the Köppen–Geiger climate classification. Hydrology and Earth System Sciences 11, 1633–1644.
Prescott, J.R., Hutton, J.T., 1994. Cosmic ray contributions to dose rates for luminescence and ESR dating. Large depths and long-term time variations. Radiation Measurements 23, 497–500.
Prescott, J.R., Stephan, L.G., 1982. The contribution of cosmic radiation to the environmental dose for thermoluminescent dating. Latitude, altitude and depth dependences. PACT Journal (Council of Europe) 6, 17–25.
Repka, J.L., Anderson, R.S., Finkel, R.C., 1997. Cosmogenic dating of fluvial terraces, Fremont River, Utah. Earth and Planetary Science Letters 152, 59–73.
Ritter, D.F., Kochel, R.C., Miller, J.R., 2002. Process Geomorphology. McGraw-Hill, New York. 560 pp.
Rockwell, T.K., Lindvall, S., Herzberg, M., Murbach, D., Dawsaon, T., Berger, G., 2000. Paleoseismology of the Johnson Valley, Kickapoo, and Homestead Valley Faults: clustering of earthquakes in the Eastern California Shear Zone. Seismological Society of America Bulletin 90, 1200–1236.
Savage, J.C., Lisowski, N.E., King, N.E., Gross, W.K., 1994. Strain accumulation along the Laguna Salada fault, Baja California, Mexico. Journal of Geophysical Research 99, 18,109–18,116.
Siem, M.E., 1992. The structure and petrology of Sierra El Mayor, northeastern Baja California, Mexico. M.S. Thesis, San Diego State University, San Diego, 244 pp.
Siem, M.E., Gastil, R.G., 1994. Mid-Tertiary to Holocene extension associated with the development of the Sierra El Mayor metamorphic core complex, northeastern Baja California, Mexico. In: McGill, S.F., Ross, T.M. (Eds.), Geological Investigations of an Active Margin. Cordilleran Section Meeting Guidebook. Geological Society of America, Redlands, California, pp. 107–119.
Sohn, M.F., Mahan, S.A., Knott, J.R., Bowman, D.D., 2007. Luminesence ages for alluvial fan deposits in southern Death Valley: implications for climate-driven sedimentation along a tectonically active mountain front. Quaternary International 166, 49–60.
Spelz, R.M., Fletcher, J.M., Owen, L.A., Caffee, M.W., 2008. Quaternary alluvial-fan development, climate and morphologic dating of fault scarps in Laguna Salada, Baja California, Mexico. Geomorphology 102 (3–4), 578–594.
Srivastava, P., Sharma, M., Singhvi, A.K., 2003. Luminescence chronology of incision and channel pattern changes in the River Ganga, India. Geomorphology 51, 259–268.
Stokes, S., 1999. Luminescence dating applications in geomorphological research. Geomorphology 29, 153–171.
Stone, J.O., 2000. Air pressure and cosmogenic isotope production. Journal of Geophysical Research 105, 23,753–23,759.
Todd, V.R., Erskine, B.G., Morton, D.M., 1988. Metamorphic and tectonic evolution of the northern Peninsular Ranges Batholith, southern California. In: Ernst, W.G. (Ed.), Metamorphism and Crustal Evolution of the Western United States. Rubey Volume, vol. VII. Prentice-Hall, Englewood Cliffs, N.J., pp. 894–937.
Van Devender, T.R., 1977. Holocene woodlands in the southwestern deserts. Science 198, 189–192.
Vazquez-Hernandez, S., Carreno, A.L., Martin-Barajas, A., 1996. Stratigraphy and paleoenvironments of the Mio-Pliocene Imperial Formation in the eastern Laguna Salada area, Baja California, Mexico. In: Abbott, P.L., Cooper, J.D. (Eds.), Field Conference Guidebook and Volume for the Annual Convention. Pacific Section of American Association of Petroleum Geologists, San Diego, California, pp. 373–380.
Wallinga, J., 2002. Optically stimulated luminescence dating of fluvial deposits: a review. Boreas 31, 303–322.
Wells, S.G., McFadden, L.D., Dohrenwend, J.C., 1987. Influence of late Quaternary climatic changes on geomorphic and pedogenic processes on a desert piedmont, eastern Mojave Desert, California. Quaternary Research 27, 130–146.
Winkler, C.D., Kidwell, S.M., 1996. Stratigraphy of a marine rift basin: Neogene of the western Salton Trough. In: Abbott, P.L., Cooper, J.D. (Eds.), Field conference guidebook and volume for the annual convention. Pacific Section of American Association of Petroleum Geologists, San Diego, California, pp. 295–336.
Zhang, J.F., Zhou, L.P., Yue, S.Y., 2003. Dating fluvial sediments by optically stimulated luminescence: selection of equivalent doses for age calculation. Quaternary Science Reviews 22, 1123–1129.
Zimmerman, D.W., 1971. Thermoluminescence dating using fine grains from pottery. Archaeometry 13, 29–52.